iScience

CellPress
OPEN ACCESS

Article

Similar neural pathways link psychological stress and brain-age in health and multiple sclerosis

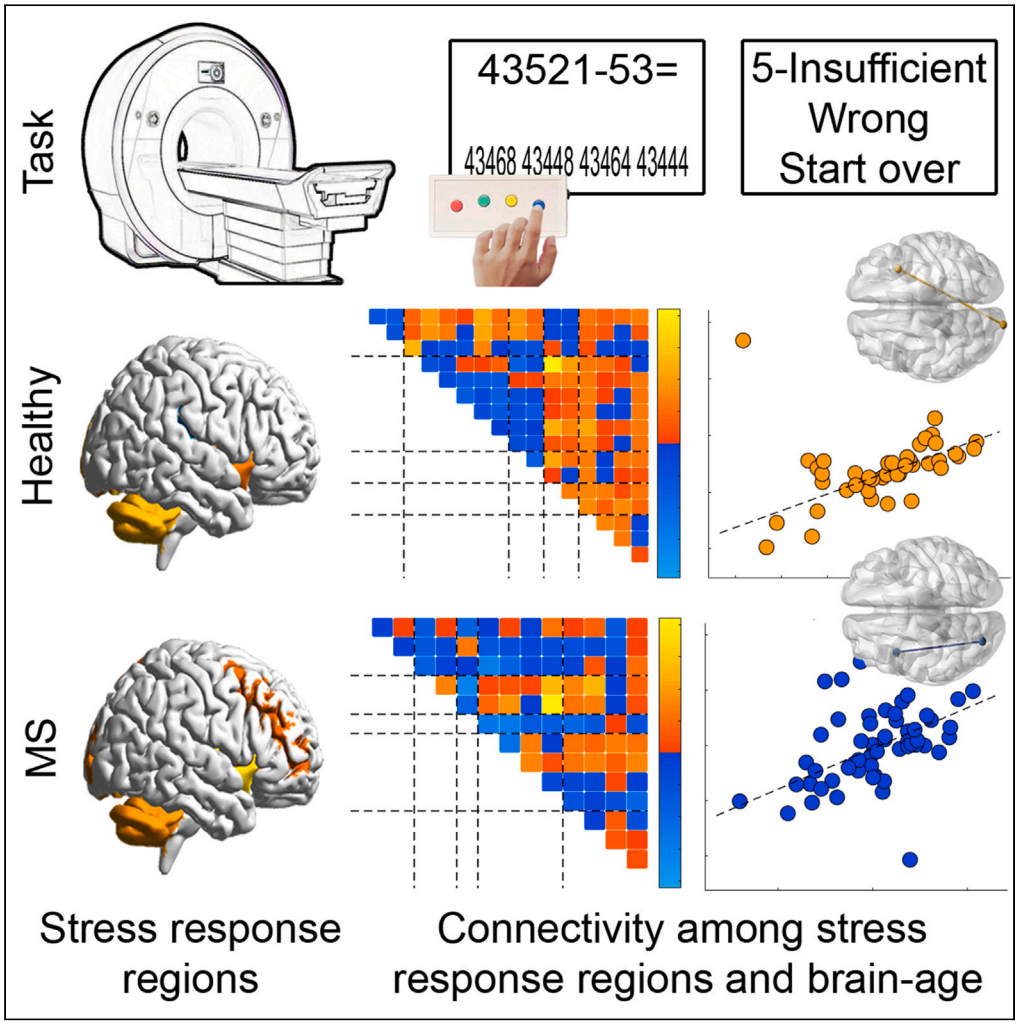

Marc-Andre Schulz, Stefan Hetzer, Fabian Eitel, ..., Friedemann Paul, Kerstin Ritter, Martin Weygandt

weygandtmartin@gmail.com

Highlights

Stress can reduce brain health in health and neurological disease including MS

It is unclear if mediating pathways are similar in healthy persons and MS patients

Insular-occipital connectivity during stress correlated with brain-age in both

This might suggest a common link between psychological stress and brain health

Schulz et al., iScience 26, 107679
September 15, 2023
https://doi.org/10.1016/j.isci.2023.107679

iScience

CellPress
OPEN ACCESS

Article

Similar neural pathways link psychological stress and brain-age in health and multiple sclerosis

Marc-Andre Schulz,[1,2,15] Stefan Hetzer,[2,3] Fabian Eitel,[1,2] Susanna Asseyer,[4,5,6,7] Lil Meyer-Arndt,[7,8,9] Tanja Schmitz-Hübsch,[4,5,6,7] Judith Bellmann-Strobl,[4,6,7] James H. Cole,[10,11] Stefan M. Gold,[12,13,14] Friedemann Paul,[4,5,6,7,16] Kerstin Ritter,[1,2,16] and Martin Weygandt[4,5,6,7,16,17,*]

SUMMARY

Clinical and neuroscientific studies suggest a link between psychological stress and reduced brain health in health and neurological disease but it is unclear whether mediating pathways are similar. Consequently, we applied an arterial-spin-labeling MRI stress task in 42 healthy persons and 56 with multiple sclerosis, and investigated regional neural stress responses, associations between functional connectivity of stress-responsive regions and the brain-age prediction error, a highly sensitive machine learning brain health biomarker, and regional brain-age constituents in both groups. Stress responsivity did not differ between groups. Although elevated brain-age prediction errors indicated worse brain health in patients, anterior insula–occipital cortex (healthy persons: occipital pole; patients: fusiform gyrus) functional connectivity correlated with brain-age prediction errors in both groups. Finally, also gray matter contributed similarly to regional brain-age across groups. These findings might suggest a common stress–brain health pathway whose impact is amplified in multiple sclerosis by disease-specific vulnerability factors.

INTRODUCTION

Converging evidence suggests that psychological stress can impair brain health – both under healthy conditions and in disease. For example, the application of stress-reducing meditation techniques is linked to better brain health in healthy humans.[1] Work on multiple sclerosis (MS) showed that brain lesion activity in persons with MS (PwMS) increases during wartime[2] and that therapeutic stress reduction can lower the occurrence of novel lesions in PwMS.[3,4] A large clinical cohort study showed that US veterans diagnosed with post-traumatic stress disorder (PTSD) have nearly double the risk of developing dementia over a seven-year period[5] and a meta-analysis that PTSD patients have reduced brain volume.[6] Consistently, stress–brain health associations were also found in invasive animal work. In healthy rodents, immobilization stress

[1]Charité – Universitätsmedizin Berlin (corporate member of Freie Universität Berlin, Humboldt-Universität zu Berlin, and Berlin Institute of Health), Department of Psychiatry and Psychotherapy, Berlin, Germany
[2]Bernstein Center for Computational Neuroscience, Berlin, Germany
[3]Charité – Universitätsmedizin Berlin, Corporate Member of Freie Universität Berlin, Humboldt-Universität zu Berlin, and Berlin Institute of Health, Berlin Center for Advanced Neuroimaging, Berlin, Germany
[4]Experimental and Clinical Research Center, A Cooperation Between the Max Delbrück Center for Molecular Medicine in the Helmholtz Association and Charité Universitätsmedizin Berlin, Berlin, Germany
[5]Charité – Universitätsmedizin Berlin, Corporate Member of Freie Universität Berlin and Humboldt-Universität zu Berlin, Experimental and Clinical Research Center, Berlin, Germany
[6]Max Delbrück Center for Molecular Medicine in the Helmholtz Association (MDC), Berlin, Germany
[7]NeuroCure Clinical Research Center, Charité – Universitätsmedizin Berlin, Corporate Member of Freie Universität Berlin and Humboldt-Universität zu Berlin, Berlin, Germany
[8]Charité – Universitätsmedizin Berlin, Corporate Member of Freie Universität Berlin, Humboldt-Universität zu Berlin, and Berlin Institute of Health, Department of Neurology, Berlin, Germany
[9]Charité – Universitätsmedizin Berlin, Corporate Member of Freie Universität Berlin, Humboldt-Universität zu Berlin, and Berlin Institute of Health, Regenerative Immunology and Aging, BIH Center for Regenerative Therapies, Berlin, Germany
[10]Centre for Medical Image Computing, Department of Computer Science, University College London, London, UK
[11]Dementia Research Centre, Institute of Neurology, University College London, London, UK
[12]Institute of Neuroimmunology and Multiple Sclerosis (INIMS), Center for Molecular Neurobiology Hamburg, University Medical Center Hamburg-Eppendorf, Hamburg, Germany
[13]Charité – Universitätsmedizin Berlin, Corporate Member of Freie Universität Berlin, Humboldt-Universität zu Berlin, and Berlin Institute of Health, Department of Psychiatry and Psychotherapy, Campus Benjamin Franklin, Berlin, Germany
[14]Charité – Universitätsmedizin Berlin, Corporate Member of Freie Universität Berlin, Humboldt-Universität zu Berlin, and Berlin Institute of Health, Medical Department, Section Psychosomatic Medicine, Berlin, Germany
[15]Department of Psychiatry, Psychotherapy, and Psychosomatics, Rheinisch-Westfälische Technische Hochschule (RWTH), Aachen University, Aachen, Germany
[16]These authors contributed equally
[17]Lead contact
*Correspondence: weygandtmartin@gmail.com
https://doi.org/10.1016/j.isci.2023.107679

reduces hippocampal neurogenesis,[7] induces irreversible dendrite loss,[8] and increases Amyloid-β peptides.[9] The experience of early life traumata induces resistance to interferon-β and neurodegeneration mediated by lymphotoxin and chemokine receptors in an animal model of MS.[10]

Given these findings, one may ask whether a common neurobiological mechanism exists that links psychological stress to reduced brain health independent of the presence of disease – a fact that could advocate the application of stress reduction for promoting brain health in health and disease alike. However, research that explicitly compares stress–brain health pathways that could potentially answer this question, is scarce. An explanation for this scarcity might be the presumption that non-invasive methods applicable in humans provide insufficient sensitivity – to measure neural stress processing, to identify meaningful brain health variations in healthy persons, or to separate disease-from age-related brain tissue variations. Neuroimaging, however, has shown that these conjectures are incorrect. Regarding the ability to measure neural stress processing, functional MRI (fMRI) has shown that psychological stress reliably correlates with specific patterns of regional brain activity (e.g., in prefrontal, limbic, insular, and occipital areas[11–13]) and their functional connectivity (FC; e.g., Maron-Katz et al.[14]). Notably, FC might be of particular importance for studying stress processing in clinical contexts, as the impact of stress can be modulated by coping strategies,[15] and the neurobiological mechanism of coping[16] as well as the preference for specific coping strategies (i.e., beneficial or detrimental for well-being) depend on FC.[17] Keeping this in mind, the specific suitability of FC for studying neurobiological stress–brain health pathways is underscored by the findings of Burns et al.,[3] who showed that the impact of stressful life events on brain lesion activity was modulated by the MS patients' subjective evaluation of (i.e., coping with) life events as either positive or negative.

With respect to the ability of measuring brain health in a non-invasive fashion, the "brain-age" paradigm which assesses brain health via "brain-predicted age differences" ("brain-PAD"[18]) has proven to fulfill the rigorous sensitivity requirements for detecting not only disease-related tissue alterations but also subclinical variations in healthy persons (HPs). Specifically, brain-PAD measures deviations from normal brain aging in terms of a formula that could be expressed as "a person's age predicted by a machine learning algorithm (i.e., their "brain-age") through a comparison of their anatomical MRI to those of a healthy reference cohort covering varying ages minus their chronological age". Algorithms accurately predicting the chronological age of HPs overestimate it (i.e., compute a positive brain-PAD) for persons with MS, dementia, mild-cognitive impairment, and schizophrenia.[19] For MS, this overestimation was replicated by a MAGNIMS consortium study,[18] which additionally showed that brain-PAD is also a biomarker for disease course prediction as higher brain-PAD goes along with shorter time-to-disability progression. Moreover, brain-PAD has sufficient sensitivity to detect meaningful brain health variations in HPs as brain-PAD links positively to mortality risk in healthy elderly,[20] and negatively to meditation practice in HPs.[1] Finally, with respect to age-related brain tissue variations, the method intrinsically controls for the impact of age on brain health given the abovementioned subtraction approach.

Despite the high individual sensitivity of FC and brain-PAD, however, these techniques have not yet been combined to compare stress–brain health pathways in HPs and neurological patients. Therefore, we employed a well-established Arterial-Spin-Labeling (ASL) fMRI stress paradigm comprising a rest and a socially evaluated mental arithmetic stress condition[11,13,21–24] to compare neurobiological pathways linking stress and brain health in 42 HPs and 56 PwMS pooled across two recent study projects (see STAR methods for details on participant selection and Methods and Figure 1 for task details). PwMS represent a group of patients well able of dealing with experimental tasks given their comparably moderate average disability and age.[25] ASL is a quantitative MRI method reflecting functional processes via differences in the regional cerebral blood flow (rCBF; ml/100 g/min) between experimental conditions that is increasingly used for FC characterization. It is better suited for stress measurement than the alternative technique blood-oxygenation-level-dependent (BOLD) fMRI as rCBF is more robust toward temporally slow[13,26] and thus stress-like[27] signal artifacts. See the review by Chen et al.[28] and the discussion for details.

We conducted four main analyses. The first three were cross-sectional and based on all 42 HPs and 56 PwMS; the fourth was longitudinal and based on a subset of PwMS comprising 24 individuals. In main analysis 1, we evaluated *activity* differences for regions included in a brain atlas defined in the anatomical standard space of the Montreal Neurological Institute (MNI)[29] as indicators of regional stress responsivity. Specifically, we computed the regions' spatially averaged voxel rCBF timeseries for the resting and the stress condition in each HP and each PwMS and contrasted the conditions' timeseries within and between groups. We expected that regional stress responsivity would not differ between groups. In main analysis 2, we computed the *functional connectivity* for stress-responsive regions in this atlas and tested associations with brain-PAD. In particular, we computed the correlation between spatially averaged rCBF timeseries for each pair of stress-responsive regions separately for the stress and rest condition in each participant and related these parameters to brain-PAD across participants separately for each condition and group. See STAR methods and Figure 2 for a description of the utilized stress responsivity and functional connectivity modeling procedure. We expected that stress-stage FC of a similar pair of regions would be associated with brain-PAD in both groups. In main analysis 3, we evaluated associations between regional brain aging reflected by brain-age voxel markers (see STAR methods for details) and the whole-brain gray matter (GM) fraction in PwMS and HPs to test our assumption that brain-age, the endpoint of the presumed stress–brain health pathway, has comparable neurobiological constituents in both groups. Finally, in the longitudinal main analysis 4, we tested associations between resting and stress-stage FC assessed at the fMRI visit of our study and future brain-PAD variations in 24 PwMS occurring in a follow-up period and expected that stress-stage FC would contain prognostic information for future brain health.

RESULTS

Clinical and demographic participant characteristics

Ten of 56 patients in the cross-sectional dataset were treated with β-interferons, ten with dimethyl fumarate, seven with glatiramer acetate, five with teriflunomide, and nine with fingolimod. Among the 24 patients in the longitudinal dataset, four were treated at baseline with β-interferons, five with dimethyl fumarate, four with glatiramer acetate, one with teriflunomide, and five with fingolimod. Table 1 gives details.

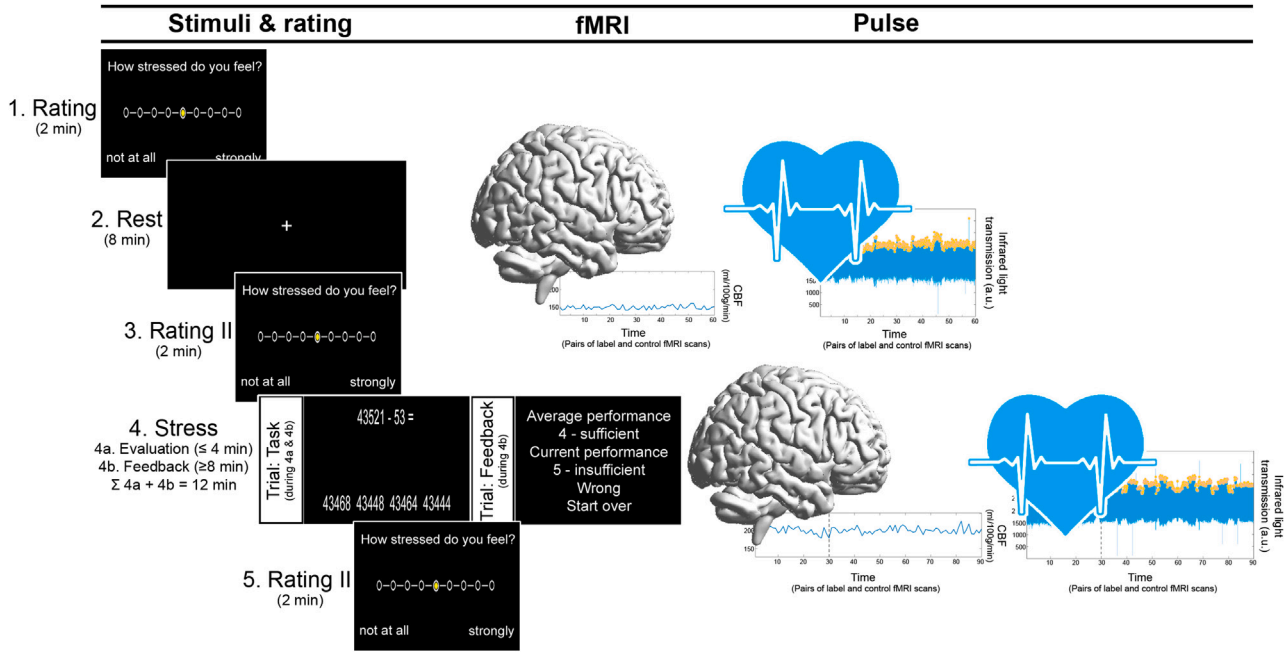

Figure 1. fMRI stress paradigm

The total paradigm comprised five stages. The stress stage was divided in stages 4a ("Evaluation") and 4b ("Feedback"). In 4a, participants performed subtraction tasks across a series of trials. In each, they had to subtract operand Y from X as fast as possible by selecting the correct answer among a set of four options depicted on a screen with an MRI-compatible response box. X started with 43521. In all trials in 4a (and 4b), operand Y was randomly determined (range: 1–99). In the first project, 4a either lasted until a participant provided ten correct answers or 4 min if they failed to provide ten correct answers. In the second, 4a had a fixed duration of 4 min. To compensate, we only evaluated rCBF, heart rate, and mental arithmetic performance data acquired in the final 8 min of 4b and modeled the duration of 4a as covariate of no interest (CNI) "time-to-feedback" in respective regression analyses in this study. In 4a, the time provided to solve a task was 8 s. When a trial was correctly solved, X equaled the difference X minus Y from the preceding trial. X remained unchanged in case of a false or too slow answer. After 4a, 4b started immediately. 4b differed in three points. First, feedback (i.e., German school grades ranging from "1 – very good" to "5 – insufficient") was provided in each trial. The grade was determined by the difference between the participant's fastest correct response in 4a and the response time of a given trial in 4b. For false or too slow answers, the feedback was always "5 – insufficient". In this case, second, X was reset to 43521. Finally, third, the time for response selection was adapted to the participant's performance. Starting with 8 s at the beginning of 4b, this time was reduced by 10% when a correct answer was provided and increased by 10% in case of false/too slow answers. This adaptive mechanism was implemented to ensure that each participant operated at the individual performance maximum across the paradigm and was thus comparable across participants from the perspective of a subjective performance norm.

Brain-age prediction accuracy and group differences in brain-PAD

The correlation between chronological and brain-age in HPs was r = 0.90 (r^2 = 0.81, p = 5.4 · 10^{-16}; mean absolute error = 6.18 [SD = 4.83] years). The average brain-PAD was 10.08 (SD = 8.99) years in patients and 3.95 (SD = 6.82) years in HPs and thus significantly higher in PwMS (t = 3.69, p = 3.7 · 10^{-4}).

Main analysis 1: Regional neural stress response activity

A wide-spread set of stress-responsive regions spanning frontal, temporal, parietal, occipital, and cerebellar areas was identified in both groups (i.e., 17 regions in HPs, 14 in PwMS). However, no group differences were found (Figure 3).

Main analysis 2: Functional connectivity and brain-PAD

We observed a significant positive association for stress-stage FC between right anterior insula and left occipital pole and brain-PAD in HPs (t = 4.22, $p_{uncorr.}$ = 4.0 · 10^{-5} = $p_{Family\text{-}Wise\text{-}Error\text{-}[FWE]\ corrected}$ = 0.005, effect size f^2 = 1.01). In PwMS, a significant positive association for FC during stress between left anterior insula and occipital fusiform gyrus and brain-PAD was found (t = 3.86, $p_{uncorr.}$ = 1.3 · 10^{-4} = p_{FWE} = 0.012, f^2 = 0.65). Resting-stage FC was neither related to brain-PAD in HPs, nor in PwMS (Figure 4).

Main analysis 3: Regional brain aging

To test whether brain-age has comparable neurobiological constituents across groups, we evaluated associations between brain-age voxel markers and the GM fraction separately in both. A strong negative association between brain-age voxel markers in parietal cortex and GM

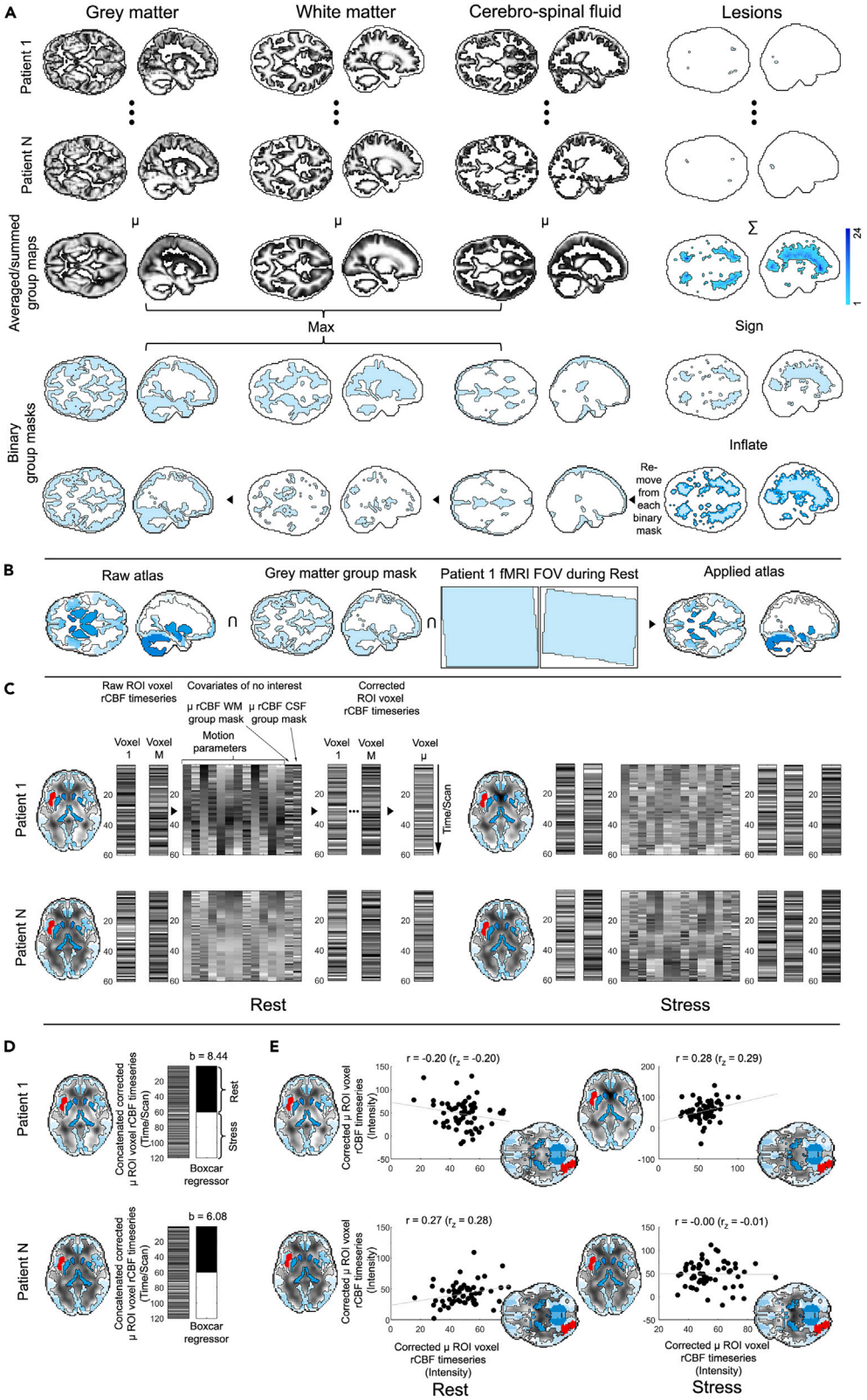
A
Grey matter
White matter
Cerebro-spinal fluid
Lesions
Patient 1
Patient N
Averaged/summed group maps
Max
Sign
Binary group masks
Inflate
Re-move from each binary mask
B
Raw atlas
Grey matter group mask
Patient 1 fMRI FOV during Rest
Applied atlas
C
Raw ROI voxel rCBF timeseries
Covariates of no interest
μ rCBF WM group mask
μ rCBF CSF group mask
Motion parameters
Corrected ROI voxel rCBF timeseries
Voxel 1
Voxel M
Voxel μ
Time/Scan
Rest
Stress
D
Concatenated corrected μ ROI voxel rCBF timeseries (Time/Scan)
b = 8.44
b = 6.08
Boxcar regressor
E
Corrected μ ROI voxel rCBF timeseries (Intensity)
r = -0.20 (r_z = -0.20)
r = 0.28 (r_z = 0.29)
r = 0.27 (r_z = 0.28)
r = -0.00 (r_z = -0.01)

Figure 2. Within-participant stress responsivity and functional connectivity modelling

(A) illustrates the computation of group masks for gray matter (GM), white matter (WM), cerebrospinal fluid (CSF), and lesions used in the fMRI analyses to constrain them to GM areas and to determine CNI. The masks were derived from voxel-wise tissue probability maps computed in the MNI standard space and manually determined lesion masks coregistered to the standard space. GM, WM and CSF tissue probability maps were first averaged across participants of a group and each voxel was classified to the tissue with the maximal averaged probability to give binary group masks for GM, WM, and CSF. For HPs, these masks were used in the fMRI analyses. In PwMS, a lesion group map was additionally computed denoting the sum of lesions per voxel across patients and coordinates with at least one lesion were classified as lesion voxel in a binary lesion mask. The binary GM, WM, and CSF group masks finally used in PwMS fMRI analyses were then determined by removing all lesion coordinates from the binary GM, WM and CSF masks determined in the step before. Importantly, however, to account for lesions in a highly sensitive fashion, we did not only remove the coordinates included in this binary lesion mask, but also coordinates with a Euclidean distance of no more than one voxel to these coordinates coded in an inflated lesion mask.

(B and C) depicts the generation of an individual and condition specific brain atlas which was defined as the intersection of the raw brain atlas, the GM group mask, and the field of view of the fMRI sequence of a given individual and condition coregistered to standard space. In 2C, the determination of averaged regional rCBF timeseries for one stress-responsive region in the individualized brain atlas, left anterior insula, is depicted for two arbitrarily selected patients and both conditions.

(D and E) illustrates the computation of left anterior insula stress responsivity (reflected by regression coefficients "b") for both patients based on concatenated averaged corrected rCBF timeseries for rest and stress. Finally, 2E shows the FC between left anterior insula and another stress-responsive region, left occipital fusiform gyrus for both patients and conditions, which is reflected by the (Fisher Z-transformed) correlation between the averaged corrected rCBF timeseries of these regions. For further details, see STAR methods and Supplement. FOV, field of view; ∩, intersection; μ, mean; ROI, region of interest; ∑, sum.

fraction was found in both groups. For HPs, the peak was located in left supramarginal gyrus at coordinate MNI: −54, −40, 38 ($t = -6.25$, $p_{FWE} = 0.012$, $f^2 = 1.15$). In other words, the higher the regional brain-age of this coordinate in an HP (i.e., the higher this coordinate biased the machine learning algorithm, a convolutional neural network [CNN], to predict an older brain-age), the lower the overall GM fraction for this HP. In PwMS, the peak coordinate was located directly adjacent in angular gyrus (MNI: −48, −57, 41; $t = -8.85$, $p_{FWE} = 0.0002$, $f^2 = 1.78$). A significant negative association in angular gyrus regions that overlapped in both groups was found at MNI: −47, −51, 44 (HPs: $t = -5.75$, $p_{FWE} = 0.041$, $f^2 = 0.97$; PwMS: $t = -6.00$, $p_{FWE} = 0.008$, $f^2 = 0.82$). To complement this analysis, we also tested associations of regional brain aging with whole-brain lesion volume in PwMS and found a strong positive association of regional brain aging with whole-brain lesion volume in periventricular white matter (WM; MNI: 33, −49, 10; $t = 8.45$, $p_{FWE} = 0.0002$, $f^2 = 1.62$). Finally, another complementary analysis testing for group differences in regional brain-age showed that PwMS were characterized by higher brain-age of right thalamus proper than HPs (MNI: 18, −27, 11; $t = 5.51$, $p_{FWE} = 0.0038$, $f^2 = 0.33$). For an illustration of these results see Figure 5, for a complete list of coordinates identified in regional brain aging analyses, see Table S1.

Main analysis 4: Functional connectivity and future brain-PAD in PwMS

This analysis showed that higher FC between right middle frontal cortex and cerebellar vermal lobule VI - VII during stress at the fMRI visit/baseline measurement in PwMS was associated with future brain-PAD increases or Δbrain-PAD respectively ($t = 4.23$, $p_{FWE} = 0.0243$; $f^2 = 2.93$; Figure 6).

DISCUSSION

Multiple findings suggest that psychological stress can impair brain health in health and disease alike. Consequently, we investigated whether comparable neurobiological stress brain-health pathways exist in health and MS with an fMRI stress task. We found that stress-stage FC between anterior insula and occipital regions was related to subclinical brain-PAD variations in HPs and to excessive brain-PAD in MS suggesting a common neurobiological pathway linking stress and brain health.

Preparatory analyses showed that prerequisites for our main analyses were fulfilled. First, brain-age prediction accuracy (interpretable for this purpose in HPs only) was high: 81% of the variance in the chronological age of HPs was explained by predicted brain-age. Second, replicating Cole et al.[18] and Kaufmann et al.,[19] patients' brain-age was overestimated compared to HPs (6.1 years on average).

Main analysis 1 tested regional neural stress responses within and between groups and showed that neural stress responses in both groups substantially overlapped with those observed in prior studies.[12,13] Consistently, an analysis presented in the supplement (Supplementary analysis 1, Figure S1) showed that the task induced a stress response in terms of heart rate and perceived stress in both groups. Crucially, however, none of the three measures differed between groups. Thus, despite findings of altered neuroendocrine stress processing in MS,[30] the basic central nervous, peripheral and psychological stress responsivity appears comparable in HPs and PwMS.

In main analysis 2, we addressed the key question of this study, whether stress-stage FC between similar stress-responsive regions is linked to brain-PAD in both groups to shed light on the assumption of a common neural pathway linking psychological stress and brain health independent of the presence of disease. As expected, main analysis 2 found that FC during stress but not rest was linked to brain-PAD in independent analyses in both groups. Further, the involved regions were similar as positive associations between stress-stage FC of anterior insula and occipital areas with brain-PAD were found for HPs as well as PwMS. Notably, involvement of anterior insular cortex in both groups might provide a hint on potential mechanisms mediating between stress and brain health. In particular, anterior insula is a central hub linking immunological to cognitive and sensory processes[31] for example realized by fusiform gyrus which (among others) serves as a screening device for biologically relevant (e.g., stress-inducing or threat-signaling) stimuli.[32] Anterior insula can be directly modulated by stress hormone administration[33] and is of major importance for measuring stress-related peripheral inflammation in HPs.[34] Recently, Koren et al.[35] showed

Table 1. Demographic, clinical and neuroradiographic participant characteristics

Cross-sectional dataset						Longitudinal dataset	
		Persons with MS	Healthy persons				Persons with MS
Sex (f/m)	#	37/19	28/14	χ^2 p	0.00 0.951	#	13/11
Age (yrs)	MN SD RG	46.4 10.7 22–66	44.7 15.5 21–75	t p	0.63 0.530	MN SD RG	48.3 7.6 27–62
Inf. proc. (#correct trials)	MN SD	28.1 10.9	34.1 12.0	t p	−2.60 0.011	MN SD	28.1 13.9
Inf. proc. (%correct trials)	MN SD	35.0 10.4	38.2 8.9	t p	−1.63 0.11	MN SD	36.0 13.8
BDI (pts.)	MN SD	8.3 7.4	2.6 3.0	t p	4.69 $9.1 \cdot 10^{-6}$	MN SD	7.1 5.5
GM (fract.)	MN SD	0.38 0.05	0.41 0.05	t p	−3.07 0.003	MN SD	0.41 0.04
WM (fract.)	MN SD	0.23 0.02	0.24 0.02	t p	−2.08 0.040	MN SD	0.25 0.02
T2LL (cm^3)	MD RG	931.5 $13.5–1.3 \cdot 10^4$				MD RG	730.7 $13.5–9.1 \cdot 10^3$
EDSS (pts.)	MD RG	2.5 0–6				MD RG	3.5 1–6
DD (yrs)	MN SD	12.7 8.8				MN SD	11.1 7.7
PROG (RR/SP)	#	49/7				#	18/6

#, number; BDI – Beck Depression Inventory; DD, disease duration assessed from the onset of symptoms; EDSS – Expanded Disability Status Scale; fract., fraction; Inf. proc., information processing capacity assessed in terms of the number of correctly solved mental arithmetic trials in the final 8 min of the stress stage; MD, median; PROG, denotes the presence of a progressive form of the disease; RG, range; RR, relapsing remitting; SP, secondary progressive; T2LL, T2-weighted lesion load.

in pivotal animal work that insular cortex does not only store information on peripheral inflammation but that it is also able to reactivate it - by reactivating the neuronal ensembles active during initial inflammation. Thus, up to the degree to which (peripheral) inflammation contributes to neuroinflammation and neurodegeneration (see Attfield et al.[36] for an overview) insular stress processing might contribute to variations in brain health. Finally, potential cellular endpoints of a stress–brain health pathway were described in animal work showing that immobilization stress reduces hippocampal neurogenesis[7] and induces irreversible dendrite loss in healthy rodents.[8] Additionally, immobilization and unpredictable random stress increase Amyloid-β peptides and Amyloid Precursor Protein expression.[9] Taken together, our results are in support of (1) clinical studies revealing a link between stress and neurological disease or brain health in neurological disease reflected by heterogeneous markers respectively,[3–6] and of (2) studies specifically identifying associations between stress and brain-age in HPs.[1,20] In particular, Cole et al.[20] showed that allostatic load, a peripheral measure accumulating the impact of life-time stress exposure, correlates positively with brain-PAD and Luders et al.[1] found that the brains of 50-year-old meditation practitioners (employing techniques frequently used for stress reduction such as Vipassana or Mindfulness meditation) were on average estimated to be 7.5 years younger than those of 50-year-old healthy controls. Finally, (3) they might complement these findings by providing first insights into mechanisms of a common neural pathway linking psychological stress and brain health independent of the presence of disease.

Having said that, however, it is also true that the brain-PAD related FC patterns do not overlap perfectly in both groups (FC between right anterior insula - left occipital pole is related to brain-PAD in HPs, left anterior insula – left fusiform gyrus FC in PwMS). For this reason and due to the current scarcity of studies on stress–brain health associations, further human studies would be helpful testing whether these deviations do or do not persist as well as more mechanistic animal studies evaluating stress-related insular contributions to brain health on a cellular level.

Complementing main analysis 2, we conducted two analyses in the supplement that both aimed at evaluating the relative suitability of parameters selected for stress – brain health modeling in main analysis 2. In particular, in Supplementary analysis 2 (see Figure S2 for details), we determined FC - GM fraction associations as benchmark for FC – brain-PAD associations and in Supplementary analysis 3 (see Figure S3 for details) we computed associations between regional neural stress response activity and brain-PAD for the same purpose. Supplementary analysis 2 (illustrated by Figure S2) showed that, although again stress-stage anterior insula FC showed the strongest association to GM fraction, the relations between FC and GM fraction were all weaker than those with brain-PAD and not significant on an FWE-corrected level.

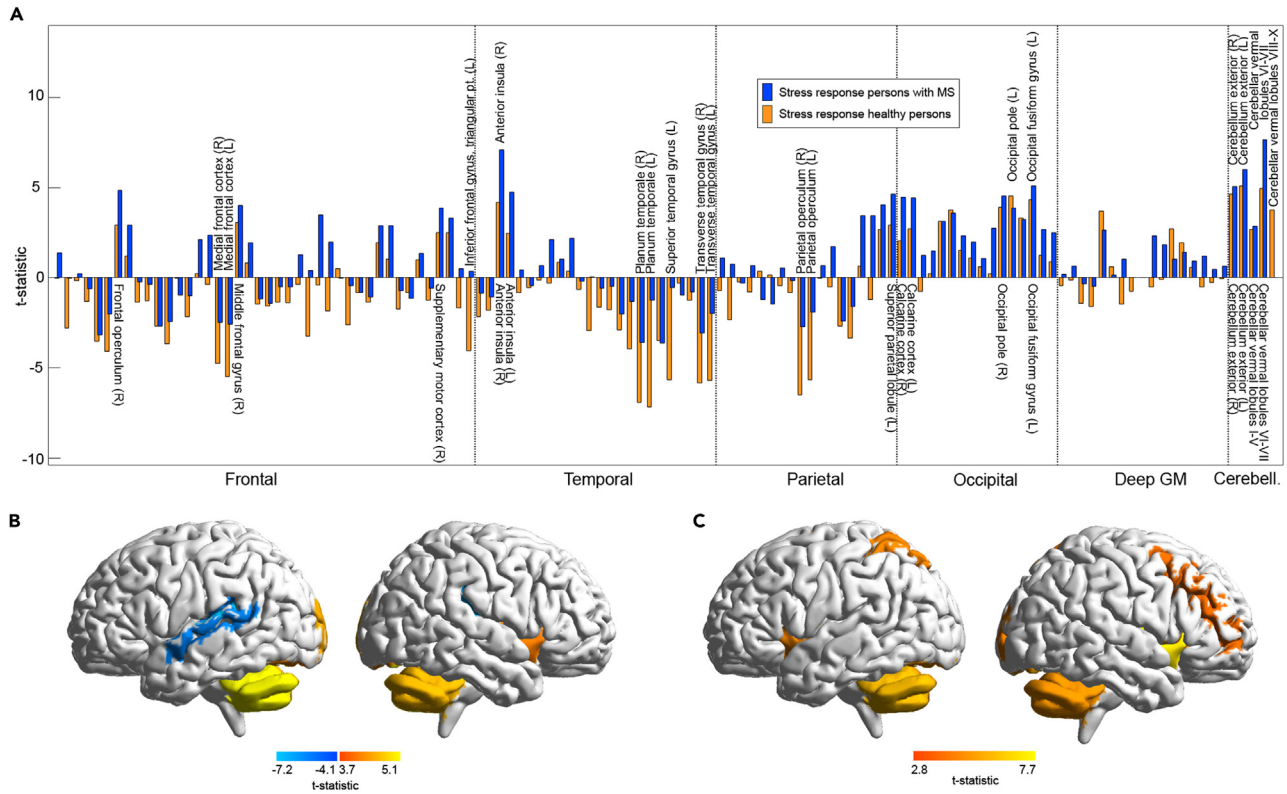

Figure 3. Neural stress responses

(A–C) shows neural stress responses. The bar graph in 3A shows the t-statistics for the difference in rCBF for stress (final 8 min of stage 4b) minus rest (stage 2) separately for both groups. Labels depicted above the baseline of 3A highlight the 17 regions yielding significant rCBF differences in HPs, labels depicted below the 14 in PwMS. Please note, that the coarse clustering of regions in 3A into frontal, temporal, etc. was conducted to increase the comprehensibility of the graph and is not necessarily optimal in anatomical terms. The render brains in 3B (HPs) and 3C (PwMS) summarize regions with significant stress responses. The scalebars in (B and C) provide the color coding for significant t-statistics obtained in the analysis of regional neural stress responsivity.

Further, also Supplementary analysis 3 (illustrated by Figure S3) failed to reveal significant associations. Together, these findings underscore the suitability of using stress-related FC assessed with ASL and brain-PAD for testing neurobiological stress – brain-health pathways.

Main analysis 3 evaluated within-group associations between regional brain aging and the whole-brain GM fraction to understand whether brain health as assessed by brain-age has comparable neurobiological constituents in both groups. Compatible with Pagani et al.[37] and Chen et al.,[38] parietal brain-age (i.e., in angular and supramarginal gyrus) showed a negative relation to patients' GM fraction (i.e., the lower a patient's GM fraction, the higher these parietal coordinates' brain-age) and a spatially overlapping negative association was found in HPs. These findings suggest that parietal over-aging might be a common marker of whole-brain GM loss and support the idea of a common pathway connecting stress as starting and brain health as endpoint. In a complementary analysis, we related regional brain aging to the whole-brain volume of hyperintense lesions which revealed a strong positive association in periventricular WM – key areas of MS lesion occurrence.[39] Moreover, we contrasted voxel-wise brain aging between groups, and, consistent with thalamic MS atrophy,[40] found that patients were characterized by elevated thalamic brain-age. Thus, the fact that one CNN model trained to predict the chronological age of HPs based on their T1-weighted scans is simultaneously sensitive to (i.e., affected in terms of age-prediction by) lesions and atrophy of PwMS in a spatially plausible fashion[39,40] suggests that brain-age computed with CNNs is a highly integrative and suitable marker of MS neuropathology. Finally, even though several studies sought to separate MS neurodegeneration from aging-related neurodegeneration (e.g., Azevedo et al.[41]), this finding also suggests that MS neuropathology has (to a certain degree) an age-like profile.

Main analysis 4 found that higher stress-stage FC between right middle frontal cortex and cerebellar vermal lobules is associated with higher future brain-PAD increases. This finding shows that stress-related FC contains prognostic information for the future course of brain health in MS. More specifically, the fact that middle frontal gyrus is a key region for modulation of stress and emotions generated in other regions including the cerebellum[16] suggests that this prognostic link relates to prefrontal stress regulation.

One aspect of the study that could be discussed is that of using ASL for investigating FC. Although it is true that the majority of FC studies still uses BOLD MRI,[28] ASL is a technique becoming increasingly popular for this purpose. Specifically, the review of Chen et al.[28] from 2015 summarizes six ASL FC studies and especially in the clinical domain a variety of additional studies have been published since then. For example, Galazzo et al.[42] (on epilepsy), Boissoneault et al.[43] (chronic fatigue syndrome), Liu et al.[44] (PTSD), and Fernandez-Seara et al.[45] (Parkinson's

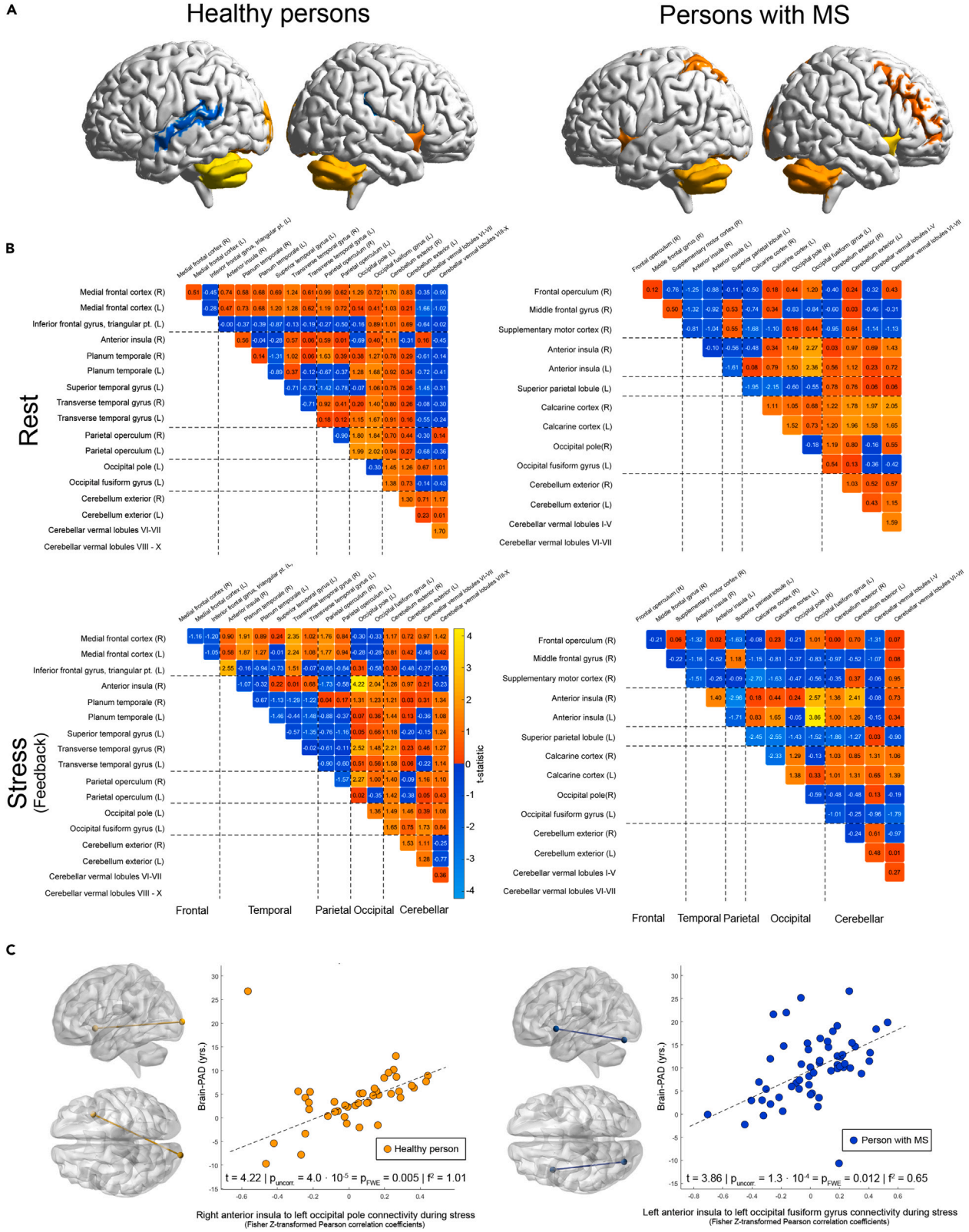
A
Healthy persons
Persons with MS
B
Rest
Stress
(Feedback)
Medial frontal cortex (R)
Medial frontal cortex (L)
Inferior frontal gyrus, triangular pt. (L)
Anterior insula (R)
Planum temporale (R)
Planum temporale (L)
Superior temporal gyrus (L)
Transverse temporal gyrus (R)
Transverse temporal gyrus (L)
Parietal operculum (R)
Parietal operculum (L)
Occipital pole (L)
Occipital fusiform gyrus (L)
Cerebellum exterior (R)
Cerebellum exterior (L)
Cerebellar vermal lobules VI-VII
Cerebellar vermal lobules VIII - X
Frontal operculum (R)
Middle frontal gyrus (R)
Supplementary motor cortex (R)
Anterior insula (R)
Anterior insula (L)
Superior parietal lobule (L)
Calcarine cortex (R)
Calcarine cortex (L)
Occipital pole(R)
Occipital fusiform gyrus (L)
Cerebellum exterior (R)
Cerebellum exterior (L)
Cerebellar vermal lobules I-V
Cerebellar vermal lobules VI-VII
t-statistic
Frontal
Temporal
Parietal
Occipital
Cerebellar
C
Brain-PAD (yrs.)
Healthy person
t = 4.22 | p_uncorr. = 4.0 · 10^-5 = p_FWE = 0.005 | f² = 1.01
Right anterior insula to left occipital pole connectivity during stress
(Fisher Z-transformed Pearson correlation coefficients)
Person with MS
t = 3.86 | p_uncorr. = 1.3 · 10^-4 = p_FWE = 0.012 | f² = 0.65
Left anterior insula to left occipital fusiform gyrus connectivity during stress
(Fisher Z-transformed Pearson correlation coefficients)

Figure 4. Functional connectivity and brain-PAD

(A) Shows stress-responsive regions identified in main analysis 1 to ease interpretability of this figure.

(B) The heatmaps in (B) depict the t-statistics for the association between FC of a given pair of stress-responsive regions on one hand and brain-PAD on the other. Specifically, the left half of (B) shows these t-statistics for HPs, the right half for PwMS. The top row shows associations for rest, the bottom row for those for stress. In the left half of (B), we illustrate (from left to right) the connection between (the center coordinates) of anterior insula and occipital regions predictive of brain-PAD and a scatter-diagram of the association between stress-related anterior insula – occipital FC and brain-PAD in HPs. In the right half of (B), we depict the same for PwMS. The scalebar in (B) provides the color coding for t-statistics obtained in the analysis of associations between FC and brain-PAD.

(C) Highlights the two regions whose FC during stress shows the strongest connection with brain-PAD separately for each group as well as the FC-brain-PAD connection in terms of a scatter-graph. The p-values reported in (C) reflect the type-I-error-rates for the strongest associations between FC and brain-PAD on an FWE-corrected level (p_{FWE}) and their uncorrected equivalents on a single test-level (p_{uncorr}).

disease). Evaluating signal detection properties of ASL FC e.g., Vallée et al.[46] found that by using standard ASL imaging protocols (i.e., 2D EPI pCASL sequence, the technique also used in our study), it was possible to detect established resting-state networks such as the default-mode and salience networks. Noteworthy, pCASL has excellent labeling efficiency and is thus the technique recommended for clinical applications by an ASL white paper.[47] Directly comparing ASL and BOLD-based FC, Jann et al.[48] report that both techniques identified common resting-state functional networks which regionally overlapped on a moderate-to-high level. This study also found that reliability for networks identified with BOLD fMRI was higher than that for ASL-derived networks which still had a sufficient reliability. This seeming disadvantage might, however, be more than compensated for by the insensitivity of ASL toward temporally slow signal artifacts[26,49] in an MS stress framework, because the neuroendocrine stress response factor which is closely related to MS and one of two major stress response components, hypothalamic-pituitary-adrenal axis-triggered glucocorticoid release, also has a slow temporal profile.[27,30,50] Consequently, whereas the removal of slow signal variation is both necessary for signal quality assurance due to the known existence of slow artifacts in BOLD fMRI and threatening to remove stress-induced signal (co)variation, slow signals can be retained unmodified in ASL fMRI.[49] Taken together, given that our ASL acquisition parameters were well within the range of the mentioned clinical ASL FC studies, given the exclusion of participants with strong head motion with the Framewise Displacement method, and the removal of motion artifacts and large-scale signal fluctuations during ASL preprocessing with regression (see STAR methods and Supplement), using ASL for studying FC in a clinical framework is an appropriate choice.

Another aspect that shall be discussed is that of potential nuisance factors which pose a considerable challenge in any observational MS study due to its multifactorial pathophysiology and frequent comorbidities in MS such as depression.[51] However, we argue that potential nuisance effects were adequately accounted for here. First, even though group differences between PwMS and HP can and in fact did occur in such parameters (e.g., in depressive symptom severity; see Table 1), these differences do not severely question the validity of our results as similar FC patterns connecting psychological stress and brain-PAD in PwMS and HPs or overlapping patterns of regional brain-age - GM fraction associations in both groups were made in independent, group-specific analyses. Further, within these group-specific analyses, a variety of potential nuisance factors were controlled for with robust regression (for example, age, sex, severity of depressive symptoms, cognitive information processing, clinical disability, disease duration, presence of a progressive disease form, time-to-feedback, and study project in main analysis 2). Moreover, the application of non-identical anatomical MRI sequences across study projects was not only accounted for by statistical modeling (a procedure also applied in multisite MS brain-age studies using different scanners such as the MAGNIMS study in which this factor accounted for 10.5% of the brain-PAD variation in patients,[18] but also by the procedure employed Bashyam et al; [52] for training their brain-age classifier. In particular, their CNN was trained on a large heterogeneous collection of neuroimaging data comprising different datasets acquired with different scanners (14,468 individuals, 12 different datasets). Finally, the most important argument in favor of our assumption of a sufficient nuisance factor consideration is again the fact that stress-related anterior insular-occipital FC was linked to brain-PAD not only in PwMS but also in HPs in independent analyses. Due to this overlap, it is unlikely that disease-specific factors not considered were driving these associations in PwMS – because disease-related factors are not present in HPs.

Conclusions

Taken together, we show that similar neural pathways link psychological stress and brain health in health and MS, which might point toward a common stress – brain health pathway. The fact that brain-PAD is higher in MS despite these similarities suggests that the effect of this association is amplified by disease-specific vulnerability factors in MS. Finally, given findings that suggest that stress modification techniques can reduce brain-PAD in HPs[1] and lesions and neurodegeneration in MS,[3,4] our study could advocate the application of stress reduction techniques for promoting brain health independent of the presence of disease.

Limitations of the study

A limitation is that the number of study participants was not precalculated in a sample size computation and that it is presumably only small to moderate when compared to clinical studies exclusively studying anatomical MRI or resting-state fMRI data. Nevertheless, we want to mention that our study rests on a large to very large sample when compared to existing MS fMRI studies using cognitive tasks according to a recent review[53] (i.e., larger than 88% when only PwMS are considered, larger than 97% when HP are also considered). Another drawback of the study is that only patients of a single neurologic disorder were investigated, which limits the findings' generalizability. Future studies should thus also include, e.g., dementia patients, despite their presumably more pronounced difficulties in participating in experimental settings given their comparably more severe average cognitive impairment.[54]

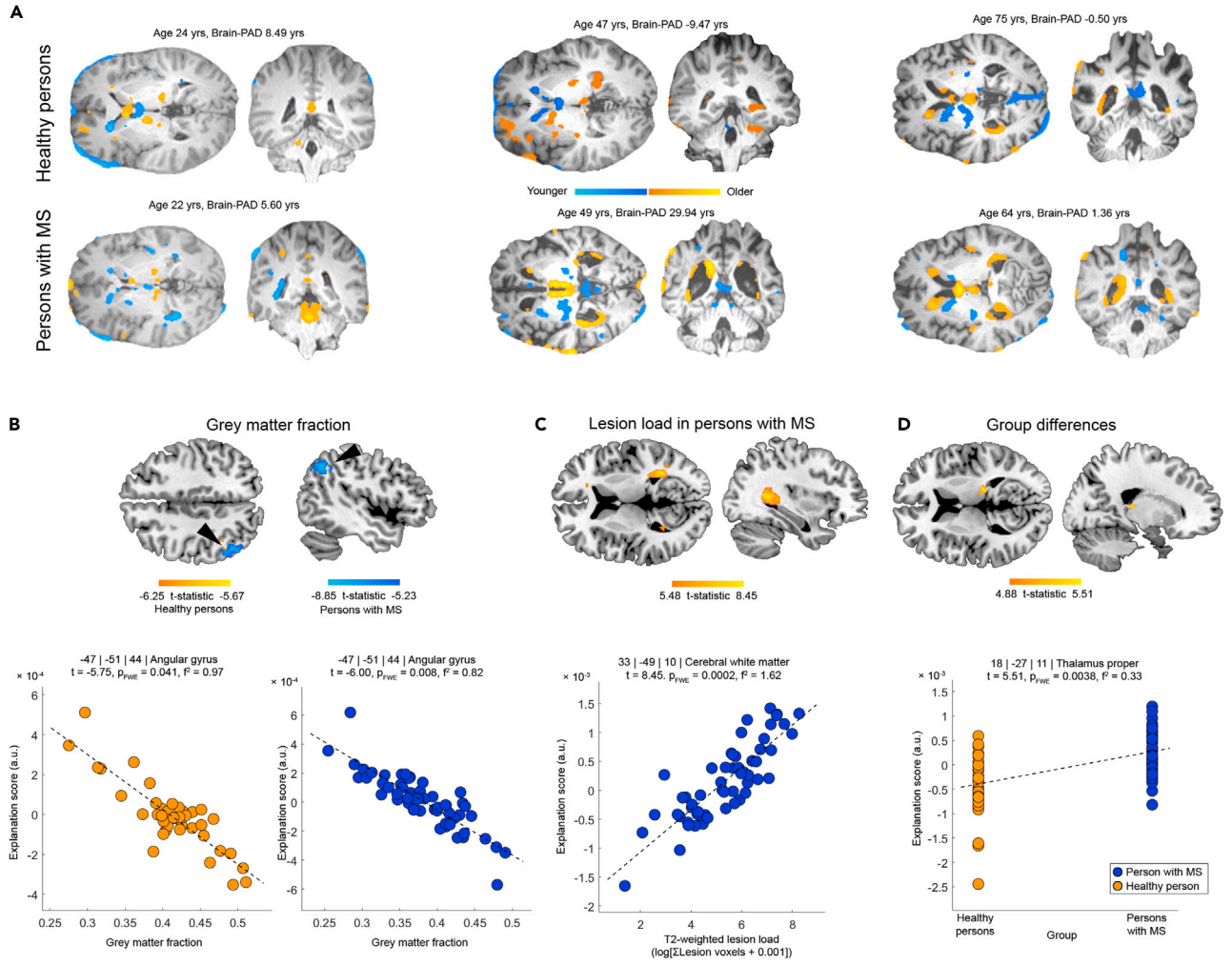

Figure 5. Regional brain aging

(A) illustrates the brain-age prediction approach or how the machine learning algorithm predicts the brain-age for six selected participants respectively. Specifically, it determines a score for each voxel which individually biases the algorithm slightly to a younger or an older age and which can be understood as marker of regional brain aging. The (weighted) sum of voxel scores gives the brain-age of a person. Voxels highlighted in blue correspond to the 5% of all voxels that contribute most strongly to a younger brain-age prediction, orange ones the 5% contributing most strongly to an older prediction. The scalebar in (A) provides the color coding for the strength of these biases.

(B) shows associations between voxel-wise brain-age scores and the whole-brain GM fraction for HPs and PwMS. In the upper row of 5B, superimposed on the axial and sagittal slices, we show significant voxel-wise t-statistics found for the link between voxel brain-age scores and GM fraction for HPs (orange palette) and for PwMS (blue palette) in independent analyses. The black arrowheads highlight the peak coordinate for which a significant negative overlapping association was found in independent analyses in both groups. The scatter graphs in the lower row of 5B illustrate the significant associations for this overlapping coordinate (i.e., at MNI: −47, −51, 44).

(C and D) presents associations between voxel-wise brain-age scores and T2-weighted lesion load in patients, 5D illustrates group differences in these scores. The scalebars in (B–D) provide the color coding for significant t-statistics obtained in (B) analysis of associations between regional brain-age and the whole-brain GM fraction or (C) whole-brain lesion load, as well as in (D) the analysis of group differences in regional brain-age. Finally, the p-values reported in (B–D) reflect the type-I-error-rates for the peak effects identified in these analyses on an FWE-corrected level.

STAR★METHODS

Detailed methods are provided in the online version of this paper and include the following:

- KEY RESOURCES TABLE
- RESOURCE AVAILABILITY
  - Lead contact
  - Materials availability

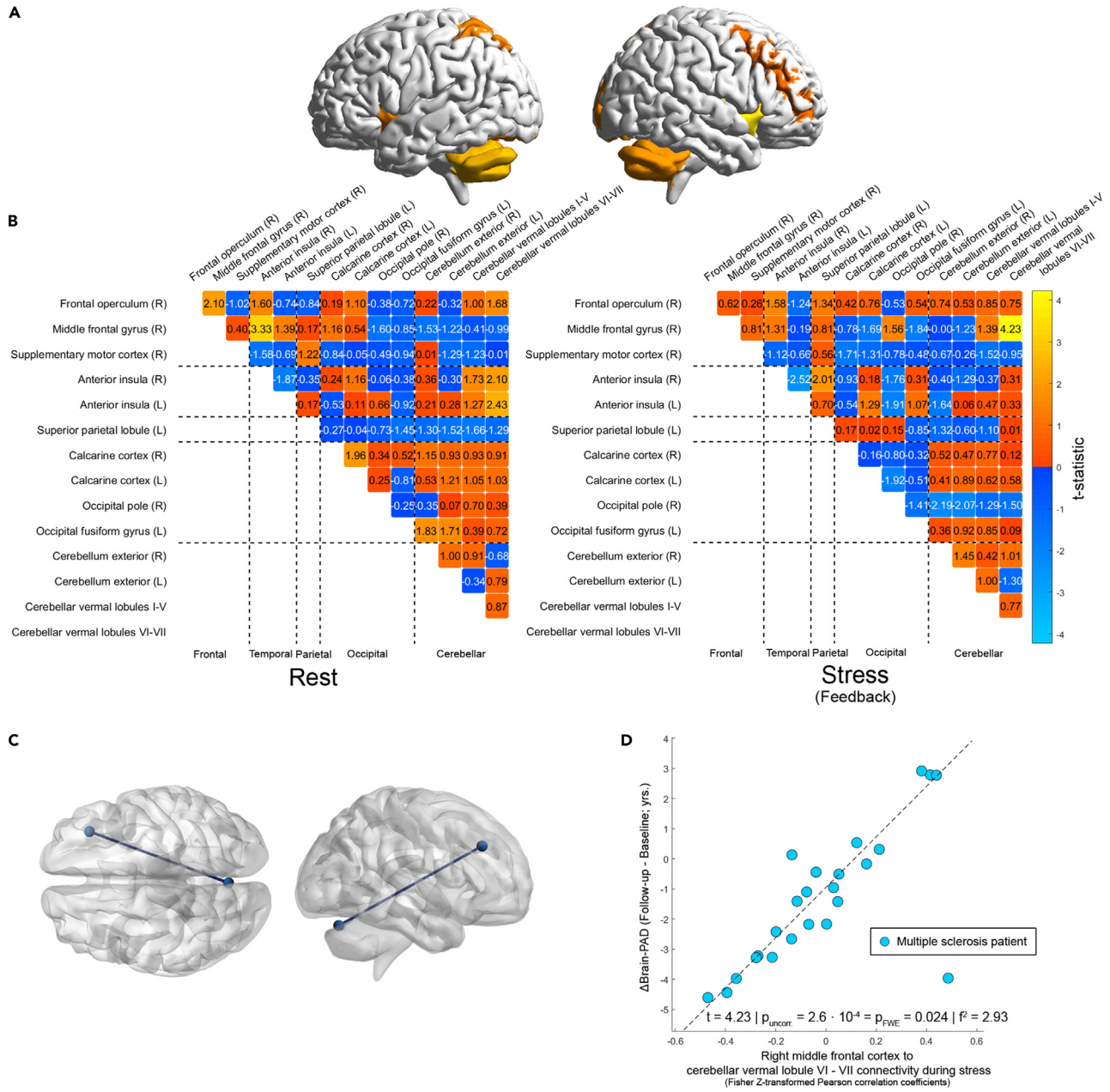

Figure 6. Functional connectivity and future brain-PAD in PwMS

(A) Shows stress-responsive regions identified in main analysis 1 to ease interpretability of this figure.

(B) The heatmaps in (B) depict the t-statistics for the association between FC at the baseline visit of pairs of stress-responsive regions and Δbrain-PAD on the left for rest and on the right for stress. The scalebar in (B) provides the color coding for t-statistics computed in the analysis of associations between FC and Δbrain-PAD.

(C) Highlights (the connection between the center coordinates of) right middle frontal cortex right and cerebellar vermal lobule VI – VII, the two regions whose stress-stage FC showed the strongest connection with Δbrain-PAD in main analysis 4.

(D) Presents a scatter-diagram of this association. The p-value reported in (D) reflects the type-I-error-rate for the strongest association between FC and Δbrain-PAD on an FWE-corrected level (p_{FWE}) and its uncorrected equivalent on a single test-level (p_{uncorr}).

SUPPLEMENTAL INFORMATION

Supplemental information can be found online at https://doi.org/10.1016/j.isci.2023.107679.

ACKNOWLEDGMENTS

We would like to thank all participants for taking part in this study and the Berlin Center for Advanced Neuroimaging for enabling the acquisition of MRI data. The work was supported by the German Research Foundation (WE 5967/2-1 and WE 5967/2-2 to MW, Exc 257 to F.P., 389563835 and CRC 1404–414984028 to K.R.), the Brain & Behavior Research Foundation (NARSAD Young Investigator Grant to K.R., USA) and the Deutsche Multiple Sklerose Gesellschaft (DMSG) eV (research award to K.R.). Our funding sources did not influence the study design, the collection, analysis and interpretation of data, the writing of the report or the decision to submit the article for publication.

AUTHOR CONTRIBUTIONS

Conceptualization, J.C. and M.W.; Investigation, S.A., L.M.A., and M.W.; Formal Analysis, M.A.S. and M.W.; Writing – Original Draft, M.A.S., S.H., F.E., T.S.H., J.B.S., J.C., S.M.G., F.P., K.R., and M.W.; Writing – Review and Editing, M.A.S. and M.W.; Visualization, M.A.S. and M.W.; Funding Acquisition, F.P., K.R., and M.W.; Resources, S.H. and M.W.; Supervision, J.C. and M.W.

DECLARATION OF INTERESTS

The authors declare no competing interests.

INCLUSION AND DIVERSITY

We support inclusive, diverse, and equitable conduct of research.

Received: October 28, 2022
Revised: July 30, 2023
Accepted: August 14, 2023
Published: August 18, 2023

REFERENCES

1. Luders, E., Cherbuin, N., and Gaser, C. (2016). Estimating brain age using high-resolution pattern recognition: Younger brains in long-term meditation practitioners. Neuroimage *134*, 508–513. https://doi.org/10.1016/j.neuroimage.2016.04.007.
2. Yamout, B., Itani, S., Hourany, R., Sibaii, A.M., and Yaghi, S. (2010). The effect of war stress on multiple sclerosis exacerbations and radiological disease activity. J. Neurol. Sci. *288*, 42–44. https://doi.org/10.1016/j.jns.2009.10.012.
3. Burns, M.N., Nawacki, E., Kwasny, M.J., Pelletier, D., and Mohr, D.C. (2014). Do positive or negative stressful events predict the development of new brain lesions in people with multiple sclerosis. Psychol. Med. *44*, 349–359. https://doi.org/10.1017/S0033291713000755.
4. Mohr, D.C., Lovera, J., Brown, T., Cohen, B., Neylan, T., Henry, R., Siddique, J., Jin, L., Daikh, D., and Pelletier, D. (2012). A randomized trial of stress management for the prevention of new brain lesions in MS. Neurology *79*, 412–419. https://doi.org/10.1212/WNL.0b013e3182616ff9.
5. Yaffe, K., Vittinghoff, E., Lindquist, K., Barnes, D., Covinsky, K.E., Neylan, T., Kluse, M., and Marmar, C. (2010). Posttraumatic Stress Disorder and Risk of Dementia. Among US Veterans. Arch. Gen. Psychiatr. *67*, 608–613. https://doi.org/10.1001/archgenpsychiatry.2010.61.
6. Bromis, K., Calem, M., Reinders, A.A.T.S., Williams, S.C.R., and Kempton, M.J. (2018). Meta-analysis of 89 structural MRI studies in post-traumatic stress disorder and comparison with major depressive disorder. Am. J. Psychiatr. *175*, 989–998. https://doi.org/10.1176/appi.ajp.2018.17111199.
7. Chetty, S., Friedman, A.R., Taravosh-Lahn, K., Kirby, E.D., Mirescu, C., Guo, F., Krupik, D., Nicholas, A., Geraghty, A., Krishnamurthy, A., et al. (2014). Stress and glucocorticoids promote oligodendrogenesis in the adult hippocampus. Mol. Psychiatry *19*, 1275–1283. https://doi.org/10.1038/mp.2013.190.
8. Radley, J.J., Rocher, A.B., Miller, M., Janssen, W.G.M., Liston, C., Hof, P.R., McEwen, B.S., and Morrison, J.H. (2006). Repeated stress induces dendritic spine loss in the rat medial prefrontal cortex. Cerebr. Cortex *16*, 313–320. https://doi.org/10.1093/cercor/bhi104.
9. Ray, B., Gaskins, D.L., Sajdyk, T.J., Spence, J.P., Fitz, S.D., Shekhar, A., and Lahiri, D.K. (2011). Restraint stress and repeated corticotrophin-releasing factor receptor activation in the amygdala both increase amyloid-beta precursor protein and amyloid-beta peptide but have divergent effects on brain-derived neurotrophic factor and pre-synaptic proteins in the prefrontal cortex of rats. Neuroscience *184*, 139–150. https://doi.org/10.1016/j.neuroscience.2011.03.067.
10. Khaw, Y.M., Majid, D., Oh, S., Kang, E., and Inoue, M. (2021). Early-life-trauma triggers interferon-ß resistance and neurodegeneration in a multiple sclerosis model via downregulated ß1-adrenergic

signaling. Nat. Commun. *12*, 105. https://doi.org/10.1038/s41467-020-20302-0.

11. Weygandt, M., Meyer-Arndt, L., Behrens, J.R., Wakonig, K., Bellmann-Strobl, J., Ritter, K., Scheel, M., Brandt, A.U., Labadie, C., Hetzer, S., et al. (2016). Stress-induced brain activity, brain atrophy, and clinical disability in Multiple Sclerosis. Proc. Natl. Acad. Sci. USA *113*, 13444–13449. https://doi.org/10.1073/pnas.1605829113.
12. Dedovic, K., Rexroth, M., Wolff, E., Duchesne, A., Scherling, C., Beaudry, T., Lue, S.D., Lord, C., Engert, V., and Pruessner, J.C. (2009). Neural correlates of processing stressful information: An event-related fMRI study. Brain Res. *1293*, 49–60. https://doi.org/10.1016/j.brainres.2009.06.044.
13. Wang, J., Rao, H., Wetmore, G.S., Furlan, P.M., Korczykowski, M., Dinges, D.F., and Detre, J.A. (2005). Perfusion functional MRI reveals cerebral blood flow pattern under psychological stress. Proc. Natl. Acad. Sci. USA *102*, 17804–17809. https://doi.org/10.1073/pnas.0503082102.
14. Maron-Katz, A., Vaisvaser, S., Lin, T., Hendler, T., and Shamir, R. (2016). A large-scale perspective on stress-induced alterations in resting-state networks. Sci. Rep. *6*, 21503. https://doi.org/10.1038/srep21503.
15. Folkman, S., and Lazarus, R.S. (1988). Coping as a mediator of emotion. J. Pers. Soc. Psychol. *54*, 466–475.
16. Ochsner, K.N., Ray, R.D., Cooper, J.C., Robertson, E.R., Chopra, S., Gabrieli, J.D.E., and Gross, J.J. (2004). For better or for worse: neural systems supporting the cognitive down- and up-regulation of negative emotion. Neuroimage *23*, 483–499. https://doi.org/10.1016/j.neuroimage.2004.06.030.
17. Santarnecchi, E., Sprugnoli, G., Mencarelli, L., Neri, F., Momi, D., DiLorenzo, G., Pascual-Leone, A., Rossi, S., and Rossi, A. (2018). Brain functional connectivity correlates of coping styles. Cogn. Affect. Behav. Neurosci. *18*, 498–508. https://doi.org/10.3758/s13415-018-0583-7.
18. Cole, J.H., Raffel, J., Friede, T., Eshaghi, A., Brownlee, W.J., Chard, D., De Stefano, N., Enzinger, C., Pirpamer, L., Filippi, M., et al. (2020). Longitudinal Assessment of Multiple Sclerosis with the Brain-Age Paradigm. Ann. Neurol. *88*, 93–105. https://doi.org/10.1002/ana.25746.
19. Kaufmann, T., van der Meer, D., Doan, N.T., Schwarz, E., Lund, M.J., Agartz, I., Alnæs, D., Barch, D.M., Baur-Streubel, R., Bertolino, A., et al. (2019). Common brain disorders are associated with heritable patterns of apparent aging of the brain. Nat. Neurosci. *22*, 1617–1623. https://doi.org/10.1038/s41593-019-0471-7.
20. Cole, J.H., Ritchie, S.J., Bastin, M.E., Valdés Hernández, M.C., Muñoz Maniega, S., Royle, N., Corley, J., Pattie, A., Harris, S.E., Zhang, Q., et al. (2018). Brain age predicts mortality. Mol. Psychiatry *23*, 1385–1392. https://doi.org/10.1038/mp.2017.62.
21. Brasanac, J., Hetzer, S., Asseyer, S., Kuchling, J., Bellmann-Strobl, J., Ritter, K., Gamradt, S., Scheel, M., Haynes, J.D., Brandt, A.U., et al. (2022). Central stress processing, T cell responsivity to stress hormones, and disease severity in multiple sclerosis. Brain Commun. *4*, fcac086. https://doi.org/10.1093/braincomms/fcac086.
22. Meyer-Arndt, L., Schmitz-Hübsch, T., Bellmann-Strobl, J., Brandt, A.U., Haynes, J.D., Gold, S.M., Paul, F., and Weygandt, M. (2021). Neural processes of psychological stress and relaxation predict the future evolution of quality of life in multiple sclerosis. Front. Neurol. *12*, 753107. https://doi.org/10.3389/fneur.2021.753107.
23. Meyer-Arndt, L., Hetzer, S., Asseyer, S., Bellmann-Strobl, J., Scheel, M., Stellmann, J.P., Heesen, C., Engel, A.K., Brandt, A.U., Haynes, J.D., et al. (2020). Blunted neural and psychological stress processing predicts future grey matter atrophy in multiple sclerosis. Neurobiol. Stress *13*, 100244. https://doi.org/10.1016/j.ynstr.2020.100244.
24. Wang, J., Korczykowski, M., Rao, H., Fan, Y., Pluta, J., Gur, R.C., McEwen, B.S., and Detre, J.A. (2007). Gender difference in neural response to psychological stress. Soc. Cogn. Affect. Neurosci. *2*, 227–239. https://doi.org/10.1093/scan/nsm018.
25. Manouchehrinia, A., Westerlind, H., Kingwell, E., Zhu, F., Carruthers, R., Ramanujam, R., Ban, M., Glaser, A., Sawcer, S., Tremlett, H., and Hillert, J. (2017). Age related multiple sclerosis severity score: disability ranked by age. Mult. Scler. *23*, 1938–1946. https://doi.org/10.1177/1352458517690618.
26. Wang, J., Aguirre, G.K., Kimberg, D.Y., Roc, A.C., Li, L., and Detre, J.A. (2003). Arterial spin labeling perfusion fMRI with very low task frequency. Magn. Reson. Med. *49*, 796–802. https://doi.org/10.1002/mrm.10437.
27. Kirschbaum, C., Pirke, K.M., and Hellhammer, D.H. (1993). The 'Trier Social Stress Test'-a tool for investigating psychobiological stress responses in a laboratory setting. Neuropsychobiology *28*, 76–81. https://doi.org/10.1159/000119004.
28. Chen, J.J., Jann, K., and Wang, D.J.J. (2015). Characterizing Resting-State Brain Function Using Arterial Spin Labeling. Brain Connect. *5*, 527–542. https://doi.org/10.1089/brain.2015.0344.
29. Tzourio-Mazoyer, N., Landeau, B., Papathanassiou, D., Crivello, F., Etard, O., Delcroix, N., Mazoyer, B., and Joliot, M. (2002). Automated anatomical labeling of activations in SPM using a macroscopic anatomical parcellation of the MNI MRI single-subject brain. Neuroimage *15*, 273–289. https://doi.org/10.1006/nimg.2001.0978.
30. Ysrraelit, M.C., Gaitán, M.I., Lopez, A.S., and Correale, J. (2008). Impaired Hypothalamic-Pituitary-Adrenal Axis Activity in Patients with Multiple Sclerosis. Neurology *71*, 1948–1954. https://doi.org/10.1212/01.wnl.0000336918.32695.6b.
31. Sinha, R. (2014). Disgust, Insula, Immune Signaling, and Addiction. Biol. Psychiatry *75*, 90–91. https://doi.org/10.1016/j.biopsych.2013.11.011.
32. Gomez, A., Rothkirch, M., Kaul, C., Weygandt, M., Haynes, J.D., Rees, G., and Sterzer, P. (2011). Emotion modulates the effects of endogenous attention on retinotopic visual processing. Neuroimage *57*, 1542–1551. https://doi.org/10.1016/j.neuroimage.2011.05.072.
33. Serfling, G., Buades-Rotger, M., Harbeck, B., Krämer, U.M., and Brabant, G. (2019). The corticosteroid prednisolone increases amygdala and insula reactivity to food approach signals in healthy young men. Psychoneuroendocrinology *99*, 154–165. https://doi.org/10.1016/j.psyneuen.2018.09.007.
34. Slavich, G.M., Way, B.M., Eisenberger, N.I., and Taylor, S.E. (2010). Neural sensitivity to social rejection is associated with inflammatory responses to social stress. Proc. Natl. Acad. Sci. USA *107*, 14817–14822. https://doi.org/10.1073/pnas.1009164107.
35. Koren, T., Yifa, R., Amer, M., Krot, M., Boshnak, N., Ben-Shaanan, T.L., Azulay-Debby, H., Zalayat, I., Avishai, E., Hajjo, H., et al. (2021). Insular cortex neurons encode and retrieve specific immune responses. Cell *184*, 5902–5915.e17. https://doi.org/10.1016/j.cell.2021.10.013.
36. Attfield, K.E., Jensen, L.T., Kaufmann, M., Friese, M.A., and Fugger, L. (2022). The immunology of multiple sclerosis. Nat. Rev. Immunol. *22*, 734–750. https://doi.org/10.1038/s41577-022-00718-z.
37. Pagani, E., Rocca, M.A., Gallo, A., Rovaris, M., Martinelli, V., Comi, G., and Filippi, M. (2005). Regional brain atrophy evolves differently in patients with multiple sclerosis according to clinical phenotype. Am. J. Neuroradiol. *26*, 341–346.
38. Chen, J.T., Narayanan, S., Collins, D.L., Smith, S.M., Matthews, P.M., and Arnold, D.L. (2004). Relating neocortical pathology to disability progression in multiple sclerosis using MRI. Neuroimage *23*, 1168–1175. https://doi.org/10.1016/j.neuroimage.2004.07.046.
39. Reich, D.S., Lucchinetti, C.F., and Calabresi, P.A. (2018). Multiple Sclerosis. N. Engl. J. Med. *378*, 169–180. https://doi.org/10.1056/NEJMra1401483.
40. Azevedo, C.J., Cen, S.Y., Khadka, S., Liu, S., Kornak, J., Shi, Y., Zheng, L., Hauser, S.L., and Pelletier, D. (2018). Thalamic atrophy in multiple sclerosis: A magnetic resonance imaging marker of neurodegeneration throughout disease. Ann. Neurol. *83*, 223–234. https://doi.org/10.1002/ana.25150.
41. Azevedo, C.J., Cen, S.Y., Jaberzadeh, A., Zheng, L., Hauser, S.L., and Pelletier, D. (2019). Contribution of normal brain aging to brain atrophy in MS. Neurol. Neuroimmunol. Neuroinflamm. *6*, e616. https://doi.org/10.1212/NXI.0000000000000616.
42. Galazzo, I.B., Storti, S.F., Barnes, A., De Blasi, B., De Vita, E., Koepp, M., Duncan, J.S., Groves, A., Pizzini, F.B., Menegaz, G., et al. (2019). Arterial Spin Labeling Reveals Disrupted Brain Networks and Functional Connectivity in Drug-Resistant Temporal Epilepsy. Front. Neuroinform. *12*, 101. https://doi.org/10.3389/fninf.2018.00101.
43. Boissoneault, J., Letzen, J., Lai, S., O'Shea, A., Craggs, J., Robinson, M.E., and Staud, R. (2016). Abnormal Resting State Functional Connectivity In Patients with Chronic Fatigue Syndrome: An Arterial Spin-Labeling fMRI Study. Magn. Reson. Imaging *34*, 603–608. https://doi.org/10.1016/j.mri.2015.12.008.
44. Liu, Y., Li, B., Feng, N., Pu, H., Zhang, X., Lu, H., and Yin, H. (2016). Perfusion Deficits and Functional Connectivity Alterations in Memory-Related Regions of Patients with Post-Traumatic Stress Disorder. PLoS One *11*, e0156016. https://doi.org/10.1371/journal.pone.0156016.
45. Fernández-Seara, M.A., Mengual, E., Vidorreta, M., Castellanos, G., Irigoyen, J., Erro, E., and Pastor, M.A. (2015). Resting State Functional Connectivity of the Subthalamic Nucleus in Parkinson's Disease Assessed Using Arterial Spin-Labeled Perfusion fMRI. Hum. Brain Mapp. *36*, 1937–1950. https://doi.org/10.1002/hbm.22747.
46. Vallée, C., Maurel, P., Corouge, I., and Barillot, C. (2020). Acquisition Duration in Resting-State Arterial Spin Labeling. How Long Is Enough? Front. Neurosci. *14*, 598. https://doi.org/10.3389/fnins.2020.00598.

47. Alsop, D.C., Detre, J.A., Golay, X., Günther, M., Hendrikse, J., Hernandez-Garcia, L., Lu, H., MacIntosh, B.J., Parkes, L.M., Smits, M., et al. (2015). Recommended implementation of arterial spin-labeled perfusion MRI for clinical applications: a consensus of the ISMRM perfusion study group and the European consortium for ASL in dementia. Magn. Reson. Med. *73*, 102–116. https://doi.org/10.1002/mrm.25197.
48. Jann, K., Gee, D.G., Kilroy, E., Schwab, S., Smith, R.X., Cannon, T.D., and Wang, D.J.J. (2015). Functional connectivity in BOLD and CBF data: similarity and reliability of resting brain networks. Neuroimage *106*, 111–122. https://doi.org/10.1016/j.neuroimage.2014.11.028.
49. Aguirre, G.K., Detre, J.A., Zarahn, E., and Alsop, D.C. (2002). Experimental design and the relative sensitivity of BOLD and perfusion fMRI. Neuroimage *15*, 488–500. https://doi.org/10.1006/nimg.2001.0990.
50. Godoy, L.D., Rossignoli, M.T., Delfino-Pereira, P., Garcia-Cairasco, N., and de Lima Umeoka, E.H. (2018). A Comprehensive Overview on Stress Neurobiology: Basic Concepts and Clinical Implications. Front. Behav. Neurosci. *12*, 127. https://doi.org/10.3389/fnbeh.2018.00127.
51. Boeschoten, R.E., Braamse, A.M.J., Beekman, A.T.F., Cuijpers, P., van Oppen, P., Dekker, J., and Uitdehaag, B.M.J. (2017). Prevalence of depression and anxiety in Multiple Sclerosis: A systematic review and meta-analysis. J. Neurol. Sci. *372*, 331–341. https://doi.org/10.1016/j.jns.2016.11.067.
52. Bashyam, V.M., Erus, G., Doshi, J., Habes, M., Nasrallah, I., Truelove-Hill, M., Srinivasan, D., Mamourian, L., Pomponio, R., Fan, Y., et al. (2020). MRI signatures of brain age and disease over the lifespan based on a deep brain network and 14 468 individuals worldwide. Brain *143*, 2312–2324. https://doi.org/10.1093/brain/awaa160.
53. Rocca, M.A., Schoonheim, M.M., Valsasina, P., Geurts, J.J.G., and Filippi, M. (2022). Task- and resting state fMRi studies in multiple sclerosis: from regions to systems and time-varying analysis. Current status and future perspective. Neuroimage. Clin. *35*, 103076. https://doi.org/10.1016/j.nicl.2022.103076.
54. Hugo, J., and Ganguli, M. (2014). Dementia and cognitive impairment: Epidemiology, diagnosis, and treatment. Clin. Geriatr. Med. *30*, 421–442. https://doi.org/10.1016/j.cger.2014.04.001.
55. Ruthotto, L., Kugel, H., Olesch, J., Fischer, B., Modersitzki, J., Burger, M., and Wolters, C.H. (2012). Diffeomorphic Susceptibility Artefact Correction of Diffusion-Weighted Magnetic Resonance Images. Phys. Med. Biol. *57*, 5715–5731. https://doi.org/10.1088/0031-9155/57/18/5715.
56. Wang, Z., Aguirre, G.K., Rao, H., Wang, J., Fernández-Seara, M.A., Childress, A.R., and Detre, J.A. (2008). Empirical optimization of ASL data analysis using an ASL data processing toolbox: ASLtbx. Magn. Reson. Imaging *26*, 261–269. https://doi.org/10.1016/j.mri.2007.07.003.
57. Nichols, T.E., and Holmes, A.P. (2002). Nonparametric Analysis of PET functional Neuroimaging Experiments: A Primer. Hum. Brain Mapp. *15*, 1–25. https://doi.org/10.1002/hbm.1058.
58. Lundberg, S.M., and Lee, S.I. (2017). A Unified Approach to Interpreting Model Predictions. Adv. Neural Inf. Process. *30*, 4765–4774.
59. Lucena, O., Souza, R., Rittner, L., Frayne, R., and Lotufo, R. (2019). Convolutional neural networks for skull-stripping in brain MR imaging using silver standard masks. Artif. Intell. Med. *98*, 48–58. https://doi.org/10.1016/j.artmed.2019.06.008.
60. Polman, C.H., Reingold, S.C., Banwell, B., Clanet, M., Cohen, J.A., Filippi, M., Fujihara, K., Havrdova, E., Hutchinson, M., Kappos, L., et al. (2011). Diagnostic criteria for multiple sclerosis: 2010 revisions to the McDonald criteria. Ann. Neurol. *69*, 292–302. https://doi.org/10.1002/ana.22366.
61. Power, J.D., Mitra, A., Laumann, T.O., Snyder, A.Z., Schlaggar, B.L., and Petersen, S.E. (2014). Methods to detect, characterize, and remove motion artifact in resting state fMRI. Neuroimage *84*, 320–341. https://doi.org/10.1016/j.neuroimage.2013.08.048.
62. Kurtzke, J.F. (1983). Rating neurologic impairment in multiple sclerosis: An expanded disability status scale (EDSS). Neurology *33*, 1444–1452. https://doi.org/10.1212/wnl.33.11.1444.
63. Hautzinger, M., Keller, F., and Kuhner, C. (2009). BDI-II: Beck-Depressions-Inventar, 2nd Edition (Pearson Assessment).
64. Beck, A.T., Ward, C.H., Mendelson, M., Mock, J., and Erbaugh, J. (1961). An inventory for measuring depression. Arch. Gen. Psychiatr. *4*, 561–571. https://doi.org/10.1001/archpsyc.1961.01710120031004.
65. Weygandt, M., Wakonig, K., Behrens, J., Meyer-Arndt, L., Söder, E., Brandt, A.U., Bellmann-Strobl, J., Ruprecht, K., Gold, S.M., Haynes, J.D., and Paul, F. (2018). Brain activity, regional grey matter loss, and decision-making in Multiple Sclerosis. Mult. Scler. *24*, 1163–1173. https://doi.org/10.1177/1352458517717089.
66. Arnemann, K.L., Chen, A.J.W., Novakovic-Agopian, T., Gratton, C., Nomura, E.M., and D'Esposito, M. (2015). Functional brain network modularity predicts response to cognitive training after brain injury. Neurology *84*, 1568–1574. https://doi.org/10.1212/WNL.0000000000001476.
67. Wang, Z. (2012). Improving cerebral blood flow quantification for arterial spin labeled perfusion MRI by removing residual motion artifacts and global signal fluctuations. Magn. Reson. Imaging *30*, 1409–1415. https://doi.org/10.1016/j.mri.2012.05.004.
68. Droby, A., Thaler, A., Giladi, N., Hutchison, R.M., Mirelman, A., Ben Bashat, D., and Artzi, M. (2021). Whole brain and deep gray matter structure segmentation: Quantitative comparison between MPRAGE and MP2RAGE sequences. PLoS One *16*, e0254597. https://doi.org/10.1371/journal.pone.0254597.
69. Cohen, J. (1988). Statistical Power Analysis for the Behavioral Sciences, 2nd ed. (Lawrence Erlbaum Associates). https://doi.org/10.4324/9780203771587.

STAR★METHODS

KEY RESOURCES TABLE

REAGENT or RESOURCE	SOURCE	IDENTIFIER
Software and algorithms		
MATLAB	MathWorks, Natick, Massachusetts, USA	https://www.mathworks.com
SPM12	Wellcome Trust Center for Neuroimaging, Institute of Neurology, UCL, London UK	http://www.fil.ion.ucl.ac.uk/spm
Python	Python Software Foundation	https://www.python.org/
Brain-age CNN model	Bashyam et al.[52]	https://github.com/vishnubashyam/DeepBrainNet
ACID	Ruthotto et al.[55]	http://diffusiontools.com/
ASLtbx	Wang et al.[56]	https://cfn.upenn.edu/zewang/ASLtbx.php
SnPM13	Nichols & Holmes[57]	http://www.nisox.org/Software/SnPM13/
Shapley Additive exPlanations toolbox	Lundberg et al.[58]	https://github.com/slundberg/shap
CONSNet skull stripping algorithm	Lucena et al.[59]	https://github.com/MICLab-Unicamp/CONSNet

RESOURCE AVAILABILITY

Lead contact

Further information and requests for any resources should be directed to and will be evaluated by the lead contact, Dr. Martin Weygandt (weygandtmartin@gmail.com) to determine whether they can be made available on a case-by case basis without identifiers.

Materials availability

The study did not generate new unique reagents.

Data and code availability

- Access to all data will be granted by the lead contact on request depending on the approval by the ethics committee and under a formal Data Sharing Agreement.
- This paper does not report original code.
- Any additional information required to reanalyze the data reported in this paper is available from the lead contact upon request.

EXPERIMENTAL MODEL AND STUDY PARTICIPANT DETAILS

Participants

The study integrates data from two independent study projects conducted by the NeuroCure and the Experimental and Clinical Research Center at Charité – Universitätsmedizin Berlin, Germany. It comprises a cross-sectional study arm (relying on a single baseline visit during which functional and anatomical MRI scans were acquired once; main analyses 1–3) and a longitudinal one (additionally comprising a follow-up visit during which anatomical scans were acquired for a second time; main analysis 4). For the three cross-sectional main analyses 1–3, stress fMRI data acquired in the first project and presented in Weygandt et al.[11] and acquired in the second project and presented in Brasanac et al.[21] were pooled. The longitudinal main analysis 4 was based on stress fMRI data acquired in the first project and presented in Meyer-Arndt et al.[23]

Clinical patient inclusion and exclusion criteria were comparable across projects: Meeting the 2010 McDonald Criteria[60] for relapsing-remitting or secondary-progressive MS (first project) or those for relapsing-remitting MS (second project). Patients had to receive a stable disease-modifying treatment for at least six (first project) or three (second project) months or no disease-modifying treatment in these periods. Finally, they had to be $\geq$18 years of age and the capabilities to use the experimental devices without restrictions. In both projects, patients were excluded if they had an additional neurologic disorder, MRI contraindications including pregnancy, an acute relapse, if they received steroid treatment in the last four weeks or in case of a known psychiatric diagnosis (first project) or when a psychiatric disorder other than a depressive or anxiety disorder was diagnosed by an experienced psychotherapist (second project). If applicable, these inclusion and exclusion criteria were identical for HPs in both projects. Next, participants were excluded for whom an insufficient anatomical image quality was determined by visual assessment conducted by M.W. Afterward, we conducted another quality assurance step and excluded participants showing pronounced fMRI head motion according to the Framewise Displacement (FWD) metric.[61] In particular, using the head motion parameters computed during fMRI preprocessing and the algorithm provided by Powers et al.,[61] we determined a single FWD summary score for each participant and both conditions (i.e., rest and stress) that characterizes all individual images acquired during the ASL measurement of

a participant and condition. Then, we determined outliers based on these summary scores separately across participants of each of the three source-studies (Weygandt et al.,[11] Brasanac et al; ,[21] and Meyer-Arndt et al; [23]) and both conditions. Specifically, when an FWD-score of a participant of a source-study and condition was more extreme than the first [third] quartile minus [plus] 1.5 times the Inter-Quartile Range of the FWD-scores computed for this source-study and condition, it was considered an outlier. Only those participants of a source-study passed the procedure who had non-outlier FWD-scores in both conditions. Finally, the data entered into the cross-sectional main analyses 1–3 were determined by excluding the data acquired in the first project (the project with slightly lower anatomical MRI resolution) of those persons who participated in both projects to avoid mixing up within- and between-subject variation and by pooling the remaining data which resulted in a set of 98 participants (56 PwMS, 42 HPs). Except for pooling, the steps were identical for longitudinal main analysis 4 and lead to an inclusion of 24 PwMS (this was a PwMS-only analysis). The flowchart in the below figure summarizes the procedure and reports participant numbers.

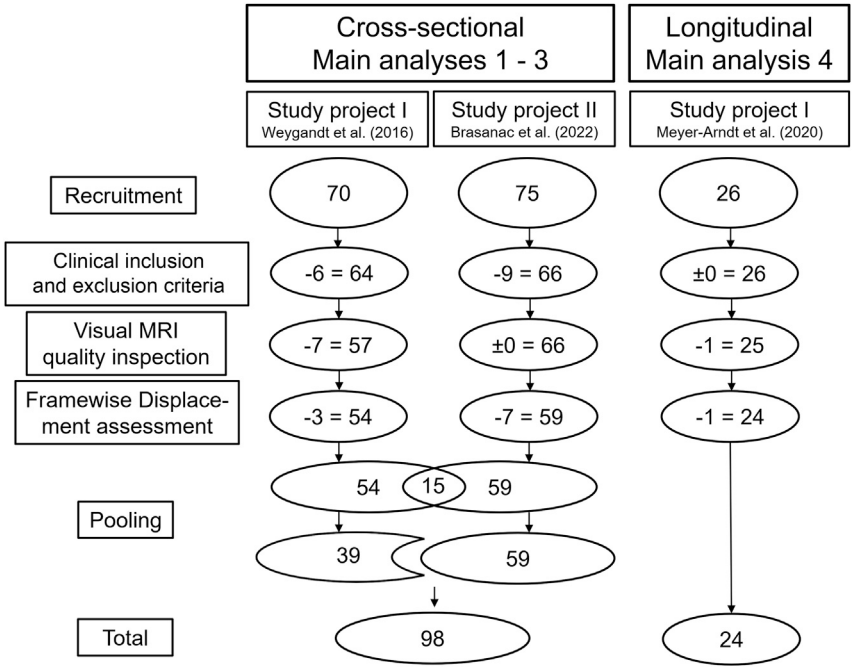

For the 24 PwMS of longitudinal main analysis 4, the median delay between the baseline and the follow-up visit was 1017 (range 717–1439) days. Both projects were conducted in accordance the Helsinki Declaration of 1975 and approved by the ethics committee of Charité – Universitätsmedizin Berlin (first project: EA1/182/10, amendment V; second: EA1/208/16). Written informed consent was obtained from all participants at all time points. Please note, that another longitudinal analysis of fMRI stress data acquired in the first study project was presented in Meyer-Arndt et al.[22]

Clinical assessments

To quantify clinical disability, the clinician-based Expanded Disability Status Scale (EDSS[62]) was used which ranges from 0 ("Normal neurological exam") to 10 ("Death due to MS"). To quantify the severity of depressive symptoms, the Beck-Depression Inventory (BDI) was used (first project BDI-II,[63] second project BDI-I[64]). Both instrument versions have 21 items with individual scores ranging from 0 to 3, yielding sum scores ranging from 0 (indicating "no/minimal depressive symptoms" for both instruments) to 63 (indicating "severe depressive symptoms" for both) and the data were pooled. For other measures assessed, see Weygandt et al.[65]

METHOD DETAILS

fMRI stress paradigm

In study project one, the paradigm comprised seven stages (1. Rating I, 2. Rest, 3. Rating II, 4. Stress, 5. Rating III, 6. Rest II, 7. Rating IV), in project two the first five thereof were assessed. Stress stage 4, during which participants had to conduct a series of mental arithmetic tasks, was divided in "Evaluation" (4a) and "Feedback" (4b) substages. In the present study, we evaluated the data from the first five stages consistently acquired in both projects. Perceived psychological stress was measured in the 1st, 3rd, and 5th stage (2 min duration each) via

a nine-point Likert-scale ranging from "not at all" to "strongly". ASL scans and heart rate (Supplement) were acquired in the 2nd (8 min) and 4th (12 min) stage. See also Figure 1.

MRI acquisition

All MR images were acquired with the same 3 Tesla whole-body tomograph (Magnetom Trio, Siemens, Erlangen, Germany) and standard 12-channel head coil. Two anatomical MR sequences were acquired in both projects. In the first, a T1-weighted sagittal 3D MP-RAGE sequence (176 slices; slice thickness 1.3 mm; in-plane voxel resolution 1.5 · 1.5 mm^2; TR = 1720 ms; TE = 2.34 ms; FA = 9°; FOV = 192 · 192 mm^2; matrix size = 128 × 128; duration 1 min and 43 s) and a sagittal T2-weighted sequence were acquired (176 slices; 1 mm isotropic voxels; TR = 5000 ms; TE = 502 ms; FA = 120°; FOV = 256 · 256 mm^2; matrix size = 256 · 256; 5 min and 52 s duration). In the second, a sagittal 3D MP-RAGE sequence (176 slices; 1 mm isotropic voxels; TR = 1900 ms; TE = 3.03 ms; FA = 9°; FOV = 256 · 256 mm^2; matrix size = 256 × 256; 4 min 26 s duration) and a sagittal T2-weighted FLAIR sequence (176 slices; 1 mm isotropic voxels; TR = 6000 ms; TE = 388 ms; TI = 2100 ms; FA = 120°; FOV = 256 · 256 mm^2; matrix size = 256 · 256; 7 min 44 s duration). In both projects, perfusion brain images were acquired with the same pseudo-continuous ASL (pCASL) echo-planar imaging (EPI) sequence (Wang et al., 2005) comprising 22 ascending transversal slices covering the whole brain (slice thickness 5.75 mm; 15% inter-slice gap; in-plane voxel resolution 3 · 3 mm^2; TR = 4000 ms; TE = 19 ms; FA = 90°; FOV = 192 · 192 mm^2; matrix size = 64 · 64; label duration 1.5 s, post-label delay 1.2 s; phase-encoding direction anterior to posterior). With this sequence, 60 control and 60 label ASL images were obtained in the Rest condition (8 min), while 90 control and 90 label scans were acquired in the Stress condition (12 min). Two spin-echo EPI reference volumes with opposing phase encoding directions (anterior to posterior, posterior to anterior) were acquired prior to the ASL measurements with matching readout and geometry for distortion correction.

MRI preprocessing

Anatomical scans

Two similar pipelines were applied, one for producing parameters needed in fMRI preprocessing ("Pipeline 1"), another for brain age computation ("Pipeline 2").

In particular, in Pipeline 1, a manual mapping of focal lesions in patients was performed by experienced raters based on patients' T2 or FLAIR images that was supervised by a neuroradiologist. Next, probability tissue maps for GM, WM, and CSF were determined based on MP-RAGE images with the combined spatial normalization and segmentation algorithm implemented in SPM12. Voxel coordinates located in lesioned tissue as indicated by the lesion masks generated in step one (which were coregistered to the T1-weighted images beforehand) were omitted. This yielded voxel-wise tissue probability maps in the anatomical standard space defined by the MNI which were corrected for potential effects of local deformations applied during spatial normalization. Additionally, the lesion masks coregistered to the T1-weighted images were coregistered to the MNI space for computation of tissue-specific group mask (see below) using the spatial mapping parameters determined in the combined normalization and segmentation procedure. The resulting voxel tissue probability maps were used to compute the GM fraction. Specifically, we first classified each voxel in MNI space as GM, WM of CSF by determining the maximal modulated tissue probability for a given voxel. If the coregistered lesion map contained a lesion at the voxel's coordinate, this voxel was always classified as lesion voxel. Afterward, the GM tissue fraction for each participant was computed by dividing the number of GM voxels by the sum of all intracranial voxels. Finally, group masks for GM, WM, and CSF were determined separately for PwMS in the cross-sectional study arm, for HPs in the cross-sectional study arm, and for PwMS in the longitudinal study arm. We computed the average tissue probability across all corresponding participants for each voxel and each of the three tissue types separately. Each voxel was then classified to the tissue for which the maximal average modulated probability was determined. Coordinates located in lesioned tissue in at least one participant and the six voxels located in direct vicinity to such coordinates (i.e., with a Euclidean distance of no more than voxel) were removed from the group masks to account for partial voluming effects.

In Pipeline 2, we matched the less complex SPM12 normalization preprocessing applied by Bashyam et al.,[52] who provided the pre-trained CNN for brain-age computation. Specifically, we spatially normalized the T1-weighted anatomical scans and thus mapped them from participants' native to MNI-space with SPM12. Following Bashyam et al.,[52] however, this normalization exclusively used linear registration. Again, areas located in lesion tissue were omitted. Afterward, we used a recently established method for skull-stripping of normalized T1-weighted scans which employs parallel two-dimensional U-Net-based CNNs and outperforms standard algorithms.[59] The resulting images were used for brain-age computations.

Functional scans

Preprocessing was performed with the ACID[55] and the ASLtbx[56] toolboxes for SPM12. It comprised a head motion correction, correction for distortions of the main magnetic field, a coregistration to the anatomical standard space defined by the MNI (voxel resolution 3 · 3 · 3 mm^3) utilizing the spatial normalization parameters determined in preprocessing of T1-weighted anatomical images, and a spatial smoothing. From the preprocessed images, we extracted voxel-wise rCBF timeseries for the rest and stress condition separately. Preprocessing and all subsequent steps utilized data from the full 8 min of the rest and the final 8 min of the stress condition and thus relied on 60 rCBF images per condition. We focused on the final 8 min of the stress condition as these were consistently included in the "Feedback" stress-substage in all participants.

Brain-age, brain-PAD, and voxel maps of regional brain-age

A single brain-age parameter reflecting a machine learning algorithm's estimate of the chronological age of a participant was computed per participant based on their T1-weighted scan in the cross-sectional study arm. In the longitudinal arm, one brain-age parameter was computed for the T1-weighted scan acquired at baseline and one for the T1-weighted scan acquired at follow-up. Specifically, the participants' spatially normalized T1-weighted scans were skull stripped with CONSNet[59] to prepare them for brain-age computation first. Next, we used a CNN provided by Bashyam et al.[52] for brain-age prediction which was pre-trained for this purpose based on the anatomical MRI scans of 11,729 healthy persons. The CNN analyzes the individual MRI slices of a participant's brain scan and predicts the participant's age from each slice. As in Bashyam et al.,[52] the median age predicted across all slices was used as a measure of brain-age. The difference "predicted brain-age minus chronological age" served as brain-PAD marker in the cross-sectional analyses 1–3. The difference in brain-PAD computed for the follow-up time point minus for the baseline time point (i.e., Δbrain-PAD) served as marker of future brain-PAD variations in the longitudinal analysis 4. In addition to this single parameter reflecting the CNN's estimate of a participant's chronological age, we computed one voxel map per participant for main analysis 3 reflecting the local influence of each voxel on this single estimate (referred to as regional or voxel-wise brain-age measures in the following). Specifically, irrespective of whether the single estimated brain-age of a participant was low or high (i.e., whether the CNN predicted a young or old person), the individual voxel scores varied from negative to positive in each participant and equaled to the single brain-age estimate when added up. Thus, the stronger positive the score of a voxel was, the stronger this voxel pushed the single brain-age estimate toward an older age and the stronger negative, the stronger it pushed this estimate toward a younger age. Due to these properties, the individual voxel scores can be viewed as measures of regional brain-age. Computation of regional brain-age scores was performed by entering Bashyam et al.[52]'s CNN model as well as the normalized and skull stripped T1-weighted scans into the Shapley Additive exPlanations toolbox.[58] The resulting voxel maps were smoothed with a 3D Gaussian kernel (8-mm full width at half maximum).

Within-participant stress responsivity and functional connectivity modeling

To determine the regional neural stress responsivity per participant in MNI-space, we first corrected the rCBF timeseries of each voxel per participant and condition that was located in (i) a given region of a brain atlas (http://Neuromorphometrics.com), (ii) the GM mask of the participant's group, and (iii) the field of view of the participant's rest or stress ASL sequence (see Figures 2A and 2B) for covariates of no interest (CNI). Specifically, following standard procedure for FC,[56,66,67] we corrected these voxels' timeseries for (i) head motion determined by ASLtbx and (ii) the rCBF timeseries of a participant and condition averaged across voxels located in the group mask of (i) WM and (ii) CSF with linear regression. Next, we computed the average rCBF timeseries for each participant, condition, and atlas region across voxels fulfilling the abovementioned criteria as proxy measure of regional neural activity (Figure 2C). Atlas regions not including a single voxel fulfilling these criteria in one or more participants were excluded from the group's analysis. Out of 122 total atlas regions, this applied to left pallidum in HPs and left and right pallidum and to cerebellar vermal lobules VIII-X in PwMS. This coverage resulted from the weak MP-RAGE pallidal GM contrast,[68] frequent cerebellar and pallidal MS lesions,[39] and the distal inferior position of cerebellar vermal lobules VIII-X (cf. Figure 2B).

To then determine parameters of regional neural stress responsivity for each participant, we concatenated the average regional voxel time series of both conditions of a participant and computed region-wise stress responses with linear regression using the concatenated time series as dependent variable. A boxcar condition regressor coding zeros for the 60 rCBF scans included in the rest stage and ones for the 60 rCBF scans included in the final 8 min of the stress stage served as predictor[56,67] (Figure 2D). The resulting region-wise regression coefficients were entered as regional stress-responsivity markers into main analysis 1. Finally, to determine the FC of stress-responsive regions (found by main analysis 1), we computed the (Fisher Z-transformed) correlation coefficient for averaged rCBF timeseries of a given pair of stress-responsive regions separately for the rest and stress stage per participant (Figure 2E) and entered them into main analysis 2.

QUANTIFICATION AND STATISTICAL ANALYSIS

Statistical analysis

Main analysis 1: Regional neural stress response activity

We tested regional stress-rest brain activity differences within and between groups with robust linear regression with the regression coefficients mentioned above as dependent variable. Age, sex, study project, and depressive symptom severity (collectively referred to as "standard nuisance factors" in the following), cognitive task load (i.e., the average duration of the inter-trial interval in the final 8 min in the stress condition) and time-to-feedback (the duration of the "Evaluation" stress substage) were included as covariates of no interest (CNI) in both within-group analyses. In the patients' analysis, EDSS, disease duration, and the presence of a progressive disease form (y/n) were included as additional CNI. Permutation testing (10,000 permutations) was used for inference. For the patients' and between-groups analyses, an FWE-corrected significance threshold for undirected tests of $\alpha_{FWE} = 0.05$ was computed by dividing 0.05 (threshold for single test) by 119 (the number of regions consistently included in the patients' and the HPs' analysis) and thus equaled $4.2 \cdot 10^{-4}$ on a single test level. For HP, the threshold corresponded to $0.05/121 = 4.1 \cdot 10^{-4}$. Here and for all other regression-based analyses, we report effect size measures f^2 ($f^2 \geq 0.02$ weak, $f^2 \geq 0.15$ medium, and $f^2 \geq 0.25$ strong effect).[69] Analyses testing psychological (self-report data) and physiological stress responses (heart rate) are described in supplementary analysis 1 (see Figure S1 for details).

Main analysis 2: Functional connectivity and brain-PAD

We used robust linear models to regress participants' brain-PAD on resting and stress-stage FC between pairs of stress-responsive regions independently for both groups and conditions. CNI were the same as in main analysis 1. Permutation testing (10,000 permutations) and an FWE-corrected significance threshold were used to evaluate significance in undirected pair-of-region-wise tests. We defined an α_{FWE} of 0.05, which corresponded to $0.05/(17 \cdot [17–1]/2) = 3.68 \cdot 10^{-4}$ on a single test level for HPs because 17 regions with significant stress-responses were found in HPs (see results). Since 14 such regions were found in PwMS, the corresponding threshold for PwMS was $0.05/(14 \cdot [14–1]/2) = 5.49 \cdot 10^{-4}$. We conducted two related supplementary analyses. In the first (Supplementary analysis 2), we determined FC - GM fraction associations to compare them against FC – brain-PAD associations or to evaluate the relative suitability of brain-PAD for studying stress – brain health pathways respectively. In the second (Supplementary analysis 3), associations between regional neural stress response activity and brain-PAD were evaluated to test the relative suitability of FC.

Main analysis 3: Regional brain aging

To clarify whether brain-age, the presumed endpoint of the investigated stress-brain health pathway, has comparable neurobiological constituents in both groups, we tested associations between regional brain-age and the whole-brain GM fraction in both groups. Additionally, we tested associations between regional brain aging and whole-brain T2-weighted lesion load in patients and differences in regional brain aging between groups to further evaluate potential pathobiological contributors to regional brain-age. For this purpose, the regional brain-age maps were analyzed with SnPM13, an SPM12 toolbox using permutation testing (10,000 permutations) and the maximum statistic FWE-correction procedure for inference. In the within-group analyses (GM-fraction in both groups, lesion load in patients), the full set of covariates comprised the standard nuisance factors, information processing capacity (i.e., the number of correctly solved arithmetic tasks in the final 8 min in the stress condition, a parameter reciprocal to cognitive task load due to the performance-adaptive task pace), GM and WM fraction for both groups. T2-weighted lesions, EDSS, disease duration, and progressive MS were additionally modeled in PwMS. Based on the full covariate set, one analysis was conducted testing associations between brain-age voxel scores as dependent variable and GM fraction as covariate of interest in both groups separately. All other covariates served as CNI. The same was done for lesion load in patients. In the analysis of group differences, standard nuisance factors plus information processing capacity served as CNI. All analyses except for the GM fraction analyses were constrained to areas located in the intersection of the SPM12's brain mask and that of Bashyam et al.[52]; the analysis of GM fraction was additionally constrained to coordinates in a given group's GM mask. Because higher GM fraction indicates better brain health but higher brain-age and lesion load indicate worse brain health, we tested for negative associations between GM fraction and brain-age voxel scores and for positive associations regarding lesion load ($\alpha_{FWE} = 0.05$).

Main analysis 4: Functional connectivity and future brain-PAD in PwMS

We evaluated whether rest and stress-stage FC measured at the baseline visit in PwMS between the pairs of stress responsive regions is associated with future variations in brain-PAD (i.e., variations between baseline and follow-up; Δbrain-PAD). The regression model was identical to that in main analysis 2 except for the facts that (i) Δbrain-PAD served as dependent variable, and (ii) brain-PAD at baseline, and (iii) the follow-up duration were modeled as additional CNI. The significance threshold was α_{FWE} of 0.05 (i.e., $0.05/(14 \cdot [14–1]/2) = 5.49 \cdot 10^{-4}$ on a single test level) and thus identical to that in main analysis 2.